https://doi.org/10.5194/egusphere-2025-5896
Preprint. Discussion started: 4 December 2025

Large impact of extreme precipitation on projected blue-green water shares

Simon P. Heselschwerdt[1,2], Thorsten Wagener[2], Lan Wang-Erlandsson[3,4,5,6], Anna M. Ukkola[7,8], Yannis Markonis[9], Yuting Yang[10,11], and Peter Greve[1]

[1]Climate Service Center Germany (GERICS), Helmholtz-Zentrum Hereon, Hamburg, Germany
[2]Institute of Environmental Science and Geography, University of Potsdam, Potsdam, Germany
[3]Stockholm Resilience Centre, Stockholm University, Stockholm, Sweden
[4]Bolin Centre for Climate Research, Stockholm University, Stockholm, Sweden
[5]Anthropocene Laboratory, The Royal Swedish Academy of Sciences, Stockholm, Sweden
[6]Potsdam Institute for Climate Impact Research (PIK), Member of the Leibniz Association, Potsdam, Germany
[7]ARC Centre of Excellence for Climate Extremes, University of New South Wales, Sydney, NSW, Australia
[8]Climate Change Research Centre, University of New South Wales, Sydney, NSW, Australia
[9]Department of Water Resources and Environmental Modeling, Faculty of Environmental Sciences, Czech University of Life Sciences Prague, Praha - Suchdol, Czech Republic
[10]State Key Laboratory of Hydroscience and Engineering, Department of Hydraulic Engineering, Tsinghua University, Beijing, China
[11]Key Laboratory of Hydrosphere Sciences of the Ministry of Water Resources, Beijing, China

Correspondence: Simon P. Heselschwerdt (simon.heselschwerdt@hereon.de)

Abstract. Precipitation partitioning into blue and green water resources is a fundamental hydroecological process shaping freshwater availability. This partitioning is determined by interactions among climatic conditions, land surface characteristics, and vegetation dynamics, which change with rising temperatures and CO_2 concentrations. Yet, global shifts in blue and green water shares and their management implications remain uncertain. We address this knowledge gap using climate simulations to quantify the relative partitioning of precipitation into green and blue water flows and its controlling factors. Here, we show that extreme five-day precipitation primarily drives partitioning shifts, favouring larger blue water shares. This effect is independent of baseline precipitation increases and generates larger blue water shares under both drying and wetting conditions. Additionally, interactions between leaf area index and plant water-use efficiency strongly impact regional partitioning trends. Our results translate shifts in blue-green water partitioning into an impact-relevant perspective, providing actionable context for water and land management.

1 Introduction

Ongoing anthropogenic climate change and other human interventions increasingly disrupt water availability and distribution (Wada et al., 2011; Greve et al., 2014; Milly and Dunne, 2016; Wada et al., 2016). At the land surface, these disruptions interfere with precipitation partitioning, with profound implications for ecosystem functions and human water demands (Falkenmark, 2013; Falkenmark et al., 2019; Gleeson et al., 2020a). Thus, understanding global changes in precipitation partitioning is critical for guiding sustainable water management.

https://doi.org/10.5194/egusphere-2025-5896
Preprint. Discussion started: 4 December 2025

Addressing these challenges requires moving beyond the traditional blue water-centric perspective (Falkenmark and Rockström, 2010). In this regard, Falkenmark (1995) advanced resource planning by incorporating the concept of green water and by later introducing the blue and green water paradigm (Falkenmark and Rockström, 2006). Blue water encompasses aquifers, lakes, and reservoirs and sustains human activities such as drinking water supply, irrigation, and industrial processes. It further stabilises Earth systems by supporting aquatic ecosystems and influencing the planet's energy balance (Wada et al., 2017; Falkenmark et al., 2019; Gleeson et al., 2020a). Green water refers to soil moisture in the unsaturated zone. It supports land system productivity and regulates critical processes such as carbon sequestration, climate regulation, and biodiversity maintenance (Rockström and Gordon, 2001; Jackson et al., 2005; Novák and van Genuchten, 2008; Falkenmark et al., 2019; Gleeson et al., 2020a). These two resources are governed by two complementary flows: green water flow, defined as transpiration, and blue water flow, involving water movement through, e.g., rivers or groundwater.

Recent studies highlight that changes in green and blue water flows can compromise critical water functions, triggering both linear and non-linear responses within ecosystems and potentially crossing tipping points in the Earth system (Falkenmark et al., 2019; Gleeson et al., 2020a; Wang-Erlandsson et al., 2022). The resilience of the Earth system is already under threat, as green and blue water sub-boundaries have transgressed the global safe operating space defined by the planetary boundaries framework (Wang-Erlandsson et al., 2022; Richardson et al., 2023; Porkka et al., 2024; Rockström et al., 2024). Therefore, developing a comprehensive understanding of how climate change influences the global partitioning of precipitation into green and blue water flows is essential for safeguarding Earth system stability (Gleeson et al., 2020b).

Yet, complex responses to changing environmental conditions introduce uncertainty when projecting future pathways of blue-green water partitioning (Wei et al., 2025). This uncertainty is strongly linked to plants' twofold response to higher CO_2 concentrations. First, increased CO_2 levels enhance surface resistance to transpiration as plants close their stomata more frequently (Leakey et al., 2009). With all other parameters held constant, this may increase global streamflow (Idso and Brazel, 1984; Milly et al., 2005; Betts et al., 2007; Fowler et al., 2019). Similarly, higher water-use efficiency (WUE) (the ratio of plant's carbon assimilation rate to transpiration rate) increases soil-moisture retention and reduces plant water stress (Swann et al., 2016). However, reduced transpiration also diminishes atmospheric moisture recycling, impacting local precipitation and regional-scale atmospheric circulation (Betts et al., 2004; Lee et al., 2012; Skinner et al., 2017). Second, elevated CO_2 levels promote the globally observed increase in vegetation biomass through CO_2 fertilisation (Leakey et al., 2009; Zhu et al., 2016; Yang et al., 2023), which can raise latent heat fluxes, enhance terrestrial water recycling, and amplify evaporative cooling and precipitation (Spracklen et al., 2012; Forzieri et al., 2020). Yet, the corresponding rise in freshwater demand simultaneously reduces streamflow in some regions, exerting additional pressure on blue water availability (Ukkola et al., 2016; Mankin et al., 2017, 2018).

Besides plant CO_2 responses and other land surface processes, climatic factors and precipitation intensity strongly influence blue and green water flows (Trenberth, 1999; Gedney et al., 2014). Extreme precipitation events generate saturation and infiltration-excess runoff, largely depending on rainfall intensity, antecedent soil moisture, and soil infiltration capacity (Horton, 1933; Dunne and Black, 1970). As these events become more frequent under climate change, they are expected to increase blue

https://doi.org/10.5194/egusphere-2025-5896
Preprint. Discussion started: 4 December 2025

water flows (Donat et al., 2016; Yin et al., 2018; Tabari, 2020). Consistently, offline Land Surface Model (LSM) experiments demonstrate that temporal concentration of precipitation is a first-order control on projected runoff ratios (Scheff et al., 2022).

Beyond changes in total blue and green water flows, recent studies directly interrogate precipitation partitioning. Earth System Model (ESM) analyses show that increasing vegetation activity reduces runoff across about half of vegetated land (Mankin et al., 2018). Particularly in the mid-latitudes, longer and warmer growing seasons reduce runoff even where precipitation increases (Mankin et al., 2019). Regional hydrological modelling finds that green water flows historically dominate in the USA, that many lowlands are runoff-consuming sinks, and that hydrologic position within the river network strongly modulates water availability (Weiskel et al., 2014). Another regional analysis links intensified rainfall to shifts from soil storage (green water) to channelised flows (blue water), thus elevating erosion risk (Eekhout et al., 2018). Additional conceptual studies highlight that changes in catchment characteristics and processes modulate runoff fractions beyond shifts in precipitation and evaporative demand (Yang et al., 2018).

However, past studies primarily emphasise changes in blue or green water flows as separate responses to shifting hydroecological conditions, while paying little attention to precipitation partitioning and its underlying drivers at the global scale to support impact-relevant interpretation. To address this knowledge gap, we use the Blue-Green Water Share (BGWS), a metric that quantifies the relative proportion of precipitation partitioned into transpiration (green water flow) and runoff (blue water flow). Positive BGWS values indicate that a larger percentage of precipitation is partitioned towards runoff than towards transpiration, and vice versa for negative values (see Sect. 2.4). We focus on these flows as they represent key variables for understanding water availability – transpiration for terrestrial ecosystems and rainfed agriculture, and runoff for aquatic ecosystems and human water withdrawals. BGWS thus provides a clear lens to assess patterns and future changes in green and blue water availability on global to continental scales, while enabling the analysis of associated controlling factors.

In this study, we analyse the historical distribution of BGWS (1985–2014) and its projected changes under the SSP3–7.0 scenario (2071–2100 minus 1985–2014) using an ensemble of 11 ESMs participating in the Coupled Model Intercomparison Project Phase 6 (CMIP6) (Eyring et al., 2016) (Table S1). We investigate the key controlling factors behind shifts in blue–green water partitioning by relating changes in BGWS to changes in mean and extreme precipitation, atmospheric water demand, soil moisture and vegetation properties. Finally, we examine how BGWS changes co-occur with absolute changes in runoff and transpiration to provide a process-based interpretation of future blue and green water availability and to discuss the implications for water and land management in a warming, CO_2-enriched world.

2 Methods

2.1 Climate model data

We use output from 11 CMIP6 ESMs that provide the required variables for both the historical experiment and the SSP3-7.0 scenario (Eyring et al., 2016) (Table S1). SSP3-7.0 represents a regional rivalry pathway (Shared Socioeconomic Pathway 3) with a radiative forcing of 7 Wm^{-2} by 2100 (Representative Concentration Pathway 7.0) (Fujimori et al., 2017; Riahi et al., 2017). We select SSP3-7.0 because it offers the broadest availability of the variables required to compute the BGWS metric

https://doi.org/10.5194/egusphere-2025-5896
Preprint. Discussion started: 4 December 2025

and to perform the subsequent analyses. This choice is further supported by recent evidence that the warmest scenario, SSP5-8.5, is unlikely to be realised under current and projected emission trajectories (Hausfather and Peters, 2020). SSP3-7.0, as the second-highest emission scenario, is therefore particularly relevant for current climate impact assessments. However, we acknowledge that hydroecological responses are scenario-dependent (Yang et al., 2018). Given the impact focus of our analysis, we prioritise a scenario whose coupled forcings more directly inform hydroecological responses and policy-relevant outcomes than idealised experiments.

For each model, we select the ensemble member with the lowest available indices along the CMIP6 ensemble axes ("ripf": realisation, initialisation, physics and forcing; member IDs in Table S1). This approach ensures that each model contributes equally to the analysis and avoids over-representing models with a larger number of ensemble members. We analyse monthly mean output of the following variables: (1) total precipitation, *pr*; (2) near-surface air temperature, *tas*; (3) near-surface specific humidity, *huss*; (4) surface pressure, *ps*; (5) evapotranspiration, *evspsbl*; (6) transpiration, *tran*; (7) leaf area index, *lai*; (8) total-column soil moisture, *mrso*; (9) total runoff, *mrro*; and (10) gross primary productivity, *gpp*. In addition, we use daily total precipitation to calculate the extreme precipitation index RX5day (annual maximum consecutive five-day precipitation; Sect. 2.3).

We use total-column soil moisture to maximise the number of models included in the analysis. Because active soil hydrology depths differ among models, we evaluate percentage relative changes in total-column soil moisture rather than absolute values. For the historical analysis, we additionally utilise upper-soil moisture (0-10 cm), *mrsos*, for which the depth is uniform across models. However, because this shallow layer does not generally represent rooting depth, we retain total-column soil moisture for subsequent analyses.

Evaporation E is diagnosed as the non-transpirational component of evapotranspiration ET and transpiration E_t,

$$E = \mathrm{ET} - E_\mathrm{t}. \tag{1}$$

This quantity represents the flux of water from liquid and solid phases to vapour from underlying surfaces, excluding transpiration. We do not use CMIP6 evaporation variables directly because key components (e.g. *evspsblsoi*) are unavailable for many models.

2.2 Observation-based and reanalysis reference datasets

To evaluate the performance of the selected CMIP6 models in simulating the BGWS, we compare the ESM results against observation-based and reanalysis datasets. Specifically, we compute the BGWS from GPCC precipitation (Schneider et al., 2022), G-RUN runoff (Ghiggi et al., 2019), and GLEAM transpiration (Miralles et al., 2011), providing an observation-based reference for model evaluation. These datasets are derived using different methodologies: GPCC is a gauge-based precipitation dataset, G-RUN reconstructs global runoff using a machine-learning approach trained on streamflow observations, and GLEAM estimates land surface evaporation from satellite-based data, incorporating microwave soil moisture retrievals and the Priestley-Taylor equation. Due to their independent origins, these datasets are not fully consistent, as they do not ensure a closed water balance at global scale. To account for this, we also use ERA5-Land, a physically consistent reanalysis dataset providing all required variables from a single modelling framework (Muñoz-Sabater et al., 2021). However, reanalysis

https://doi.org/10.5194/egusphere-2025-5896
Preprint. Discussion started: 4 December 2025

data are not direct observations and inherit uncertainties from model physics, model parametrisations and input data quality. While ERA5-Land offers a spatially and temporally coherent dataset, its ability to accurately represent long-term hydrological changes remains uncertain (Dutta and Markonis, 2024). To ensure comparability, we apply the same data processing and methodological steps to the observation-based and reanalysis datasets as to the CMIP6 model output over the historical period.

2.3 Climate indices and derived variables

In addition to directly simulated variables, we compute three climate indices: RX5day, vapour pressure deficit (VPD) and water-use efficiency (WUE). RX5day is derived from daily precipitation as the annual maximum consecutive five-day precipitation. For a given year j,

$$\text{RX5day}_j = \max(RR_{kj}), \tag{2}$$

where RR_{kj} denotes total precipitation accumulated over any five-day interval ending on day k within year j. VPD is calculated using the Buck equation (Buck, 1981) to estimate saturation vapour pressure (e_s),

$$e_\text{s} = 611.21 \times \exp\left[\left(18.678 - \frac{T}{234.5}\right)\left(\frac{T}{257.14+T}\right)\right], \tag{3}$$

where T is near-surface air temperature in °C, and 611.21 Pa is the saturation vapour pressure at 0 °C. Actual vapour pressure (e_a) is obtained from specific humidity (q) and surface pressure (p_s, in Pa) as

$$e_\text{a} = \frac{q\,p_\text{s}}{0.622 + 0.378\,q}, \tag{4}$$

and VPD is then given by

$$\text{VPD} = e_\text{s} - e_\text{a}. \tag{5}$$

We use the ratio of gross primary productivity (GPP) to transpiration to compute water-use efficiency (WUE), a widely used proxy for the CO_2 effect on stomatal resistance (Keenan et al., 2013; Lian et al., 2021; Ruehr et al., 2023):

$$\text{WUE} = \frac{\text{GPP}}{E_\text{t}}, \tag{6}$$

which quantifies the efficiency of carbon assimilation per unit of water consumed by vegetation through transpiration.

2.4 Blue-Green Water Share metric

We select runoff as the proxy for blue water flow and transpiration as a proxy for green water flow, recognising both flows as critical indicators of the volume of precipitation allocated to the distinct water resource components. Focusing on these water flows is further justified by their direct link to blue-green water partitioning, their capacity to capture key water cycle dynamics, and the valuable insights they provide even without detailed observations of storage dynamics (Wu et al., 2021). On multi-decadal timescales (here, 30-year means), storage changes tend to be small relative to fluxes, as most catchments approach

https://doi.org/10.5194/egusphere-2025-5896
Preprint. Discussion started: 4 December 2025

approximate steady state within this period (Han et al., 2020). Neglecting storage terms therefore provides a pragmatic yet interpretable framework, though we recognise this simplification as a limitation and an avenue for future research.

The BGWS metric is defined as

$$\mathrm{BGWS} = \frac{\mathrm{Runoff} - \mathrm{Transpiration}}{\mathrm{Precipitation}} \times 100, \tag{7}$$

which yields a dimensionless index expressed in percentage. Positive BGWS values indicate a partitioning imbalance that favours blue water flows (blue water regimes), where a larger share of precipitation contributes to runoff and hence to blue water resources. Negative BGWS values indicate regimes dominated by green water (green water regimes), where a greater share of precipitation is used by terrestrial ecosystems via transpiration. BGWS can thus be interpreted as the percentage imbalance of total precipitation between blue and green water flows. A deviation of ± 10 from equilibrium corresponds to a 10 % greater allocation of precipitation towards blue or green water, respectively.

Changes in BGWS values, denoted as ΔBGWS, indicate shifts in blue-green water partitioning. We compute

$$\Delta\mathrm{BGWS} = \mathrm{BGWS}_{\mathrm{Future}} - \mathrm{BGWS}_{\mathrm{Historical}}. \tag{8}$$

A positive ΔBGWS reflects an increasing partitioning towards blue water flow, whereas a negative ΔBGWS indicates an increasing partitioning towards green water flow. Although ΔBGWS does not directly measure variations in green and blue water flows, they provide a clear depiction of the trade-off between these components.

2.5 Data preprocessing and multi-model ensemble

To enable spatial comparison across models and datasets, we regrid all fields to a common $1^\circ \times 1^\circ$ latitude–longitude grid using conservative interpolation. After regridding, we compute 30-year climatological means for a historical period (1985–2014) and a far-future period (2071–2100). BGWS is calculated for each period, and changes are then obtained as differences between future and historical values for BGWS and all other variables. We employ an unweighted multi-model ensemble (MME) to mitigate uncertainties associated with individual model biases and initial-condition variability. For each model, we first compute BGWS and variable changes at the model level and then average these to obtain the MME mean. This ordering ensures that ensemble statistics reflect individual model responses before averaging. We do not apply performance-based weighting, as our objective is to assess broad climate impacts on BGWS rather than to optimise the ensemble for a specific variable. Spatial means are always calculated as area-weighted averages to account for the convergence of meridians with latitude. Each grid cell is weighted by the cosine of its latitude, $\cos(\varphi)$, where φ denotes latitude, ensuring that higher-latitude grid cells contribute proportionally less area than equatorial grid cells.

2.6 Multiple regression analysis

Predictor variables are chosen to represent hydroecological processes relevant to climate-change impacts and to allow physical interpretation of their influence on ΔBGWS. We use changes in mean precipitation (ΔPR) and extreme precipitation (ΔRX5day) to capture long-term moisture availability and short-term hydrological extremes. Changes in vapour pressure deficit (ΔVPD)

https://doi.org/10.5194/egusphere-2025-5896
Preprint. Discussion started: 4 December 2025

represent atmospheric dryness and plant physiological stress, while changes in soil moisture (ΔSM) reflect land-surface water availability. Vegetation dynamics, including biophysical changes and CO_2 fertilisation effects, are represented by changes in leaf area index (ΔLAI), and changes in water-use efficiency (ΔWUE) describe plant physiological responses to elevated CO_2.

We construct multiple linear regression (MLR) models separately for each historical BGWS regime to assess how these hydroecological drivers affect ΔBGWS, using MME mean changes in the predictors. Prior to fitting, each predictor is scaled by its maximum absolute value (maximum scaling), such that each feature is bounded by $[-1, 1]$. The response variable ΔBGWS is left on its original scale. The dataset is split into 70 % training and 30 % testing subsets.

To address multicollinearity among predictors and to regularise the regression, we apply Elastic Net regularisation (Friedman et al., 2010). The Elastic Net objective function is

$$\min_{\boldsymbol{\beta}} \left[\frac{1}{2n} \sum_{i=1}^{n} (y_i - \hat{y}_i)^2 + \alpha\rho \sum_{j=1}^{p} |\beta_j| + \frac{\alpha(1-\rho)}{2} \sum_{j=1}^{p} \beta_j^2 \right], \tag{9}$$

where y_i and $\hat{y}_i$ are the observed and predicted values, n is the number of observations, β_j are the regression coefficients, α controls the overall regularisation strength and ρ determines the balance between L1 (Lasso) and L2 (Ridge) penalties, ranging from 0 (pure Ridge) to 1 (pure Lasso). The first term measures model fit via the residual sum of squares. The L1 penalty promotes sparsity by shrinking some coefficients to exactly zero, thereby facilitating feature selection, whereas the L2 penalty shrinks coefficients towards zero without eliminating them, helping to stabilise estimates under multicollinearity.

We select α and ρ using 5-fold cross-validation on the training data, evaluating a predefined grid of hyperparameter combinations and choosing the configuration that maximises the coefficient of determination (R^2). After selecting the optimal hyperparameters, the model is retrained on the full training dataset. Predictive performance and generalisability are then assessed on the testing subset using R^2.

To quantify the contribution of each predictor to model performance, we compute permutation importance scores (Breiman, 2001). This model-agnostic metric is obtained by randomly permuting the values of a given predictor and quantifying the resulting change in R^2. For each predictor, we perform 20 permutations in both the training and testing datasets and aggregate the corresponding importance scores. Applying the method to both training and testing data allows us to compare model behaviour on seen and unseen data. However, we primarily interpret importance scores derived from the testing data as measures of out-of-sample predictor relevance for ΔBGWS. In some cases, the decrease in R^2 associated with permuting a predictor can exceed the model's baseline R^2, indicating that the model's performance drops below that of a mean-only benchmark when the information in that predictor is destroyed. This does not imply that the model relies exclusively on a single predictor, but rather highlights its strong contribution to predictive skill.

https://doi.org/10.5194/egusphere-2025-5896
Preprint. Discussion started: 4 December 2025

3 Results

3.1 Historical distribution of the Blue-Green Water Share

Figure 1a shows the global distribution of the BGWS for the historical period (1985-2014), based on the multi-model ensemble mean. Land fractions with greater shares of blue water (blue water regime) and green water (green water regime) are equally distributed. On average, ~ 3 % more of the global land precipitation is partitioned towards blue water flow, with notable ensemble variability from -6% to +14% (Table S2). These contrasts stem from differences in the model representation of precipitation characteristics, land-surface hydrology, and vegetation dynamics (Clark et al., 2015; Gentine et al., 2019; Zheng et al., 2019; Padrón et al., 2022; Yang et al., 2023). Comparing the spatial pattern of the ensemble mean BGWS with observation-based and reanalysis products demonstrates a reasonable representation (Fig. S1). Yet, the absolute BGWS values are biased towards too much blue water. Decomposing the BGWS into runoff (Q/P) and transpiration (T/P) ratios shows that both components contribute to this bias. The ensemble mean largely underestimates T/P (negative mean offset) and modestly overestimates Q/P (positive mean offset) (Figs. S2 and S3). Accordingly, we treat BGWS as a process indicator and base interpretation on directional (sign-robust) patterns and covariation with drivers (e.g., RX5day), not on absolute levels; regions with large baseline biases are interpreted cautiously. These biases in CMIP6 land-surface water fluxes and their attribution are described in detail in the literature (e.g., Li et al., 2021; Zhang et al., 2023).

Despite these model-specific and regional variations, three overarching features of the BGWS distribution emerge: energy-limitation, water-limitation, and precipitation-intensity regulated partitioning. Energy-limitation regulated partitioning, the first BGWS feature, is dominant across higher latitudes ($> 60°$N) and high-altitude regions consistently showing greater partitioning towards blue water flow (Fig. 1a). This pattern aligns with the Budyko framework, which links energy-limited conditions to increased runoff (Budyko, 1974). In the higher latitudes, 94% of the land area exhibits a larger blue water share with a zonal mean BGWS of +40%. Here, low net radiation (light-limited) and low air temperatures (kinetic/phenology-limited) result in below-average gross primary productivity (GPP) and transpiration (Figs. 1d and S4), while near-saturated soil moisture likely persists. Consequently, precipitation predominantly contributes to surface runoff (Fig. 1b,c). Furthermore, mountain ranges exhibit distinct precipitation and runoff patterns. Here, orographically enhanced precipitation and topography-controlled runoff parametrisations in ESMs (e.g., SIMTOP) cause larger blue water shares (Niu et al., 2005; Gnann et al., 2025). Additionally, in both higher latitudes and high-altitude regions, snowmelt-driven runoff likely further enhances blue water shares (Barnett et al., 2005), although ongoing warming-related snow cover loss increases net radiation and evapotranspiration, reducing runoff (Milly and Dunne, 2020). Energy-limitation regulated partitioning is also dominant across about half of the mid-latitudinal land area (40-60°N/S). Contrary to higher latitudes, these regions show a smaller blue water share with a zonal mean BGWS of $\sim +6$ %, likely due to seasonal contrasts between winter energy limitation and summer water limitation (Knoben et al., 2018). Note that, compared with observation- and reanalysis-based products, the ensemble mean overstates both the magnitude and the spatial extent of blue water shares in energy-limited high- and mid-latitudes (Fig. S1).

https://doi.org/10.5194/egusphere-2025-5896
Preprint. Discussion started: 4 December 2025

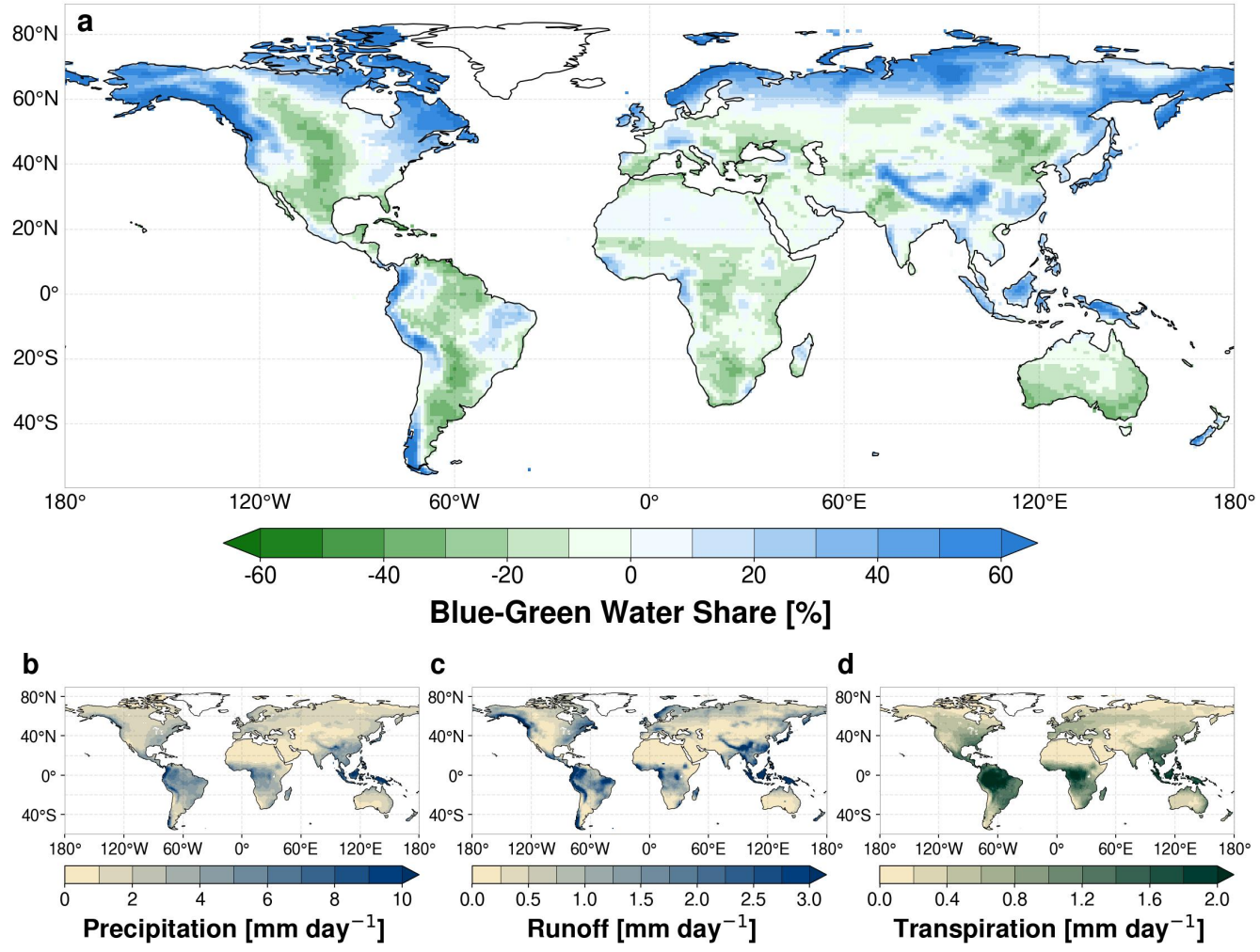

Figure 1. Ensemble mean for the historical period (1985–2014) based on 11 CMIP6 ESMs. a, Blue-Green Water Share (BGWS) [%], b, precipitation [mm day^{-1}], c, runoff [mm day^{-1}], and d, transpiration [mm day^{-1}]. Blue colours of the BGWS colourmap indicate a greater precipitation partitioning towards runoff (blue water flow) and green colours correspond to a larger partitioning towards transpiration (green water flow).

Water-limitation regulated partitioning, the second BGWS feature, dominates in global drylands such as the Eurasian Steppe or Australia's Outback (Fig. 1a). These water-limited environments are marked by annual precipitation below the global mean and relatively low soil-moisture content (Figs. 1b and S4b). Despite these hydrological constraints, these ecosystems partition a larger fraction of available water towards transpiration, increasing the green water share in line with observation-based data (Figs. 1a,d and S1). While consistently low precipitation typically favours green water dominance, infrequent but intense rainfall in dryland regions can periodically trigger high surface runoff (Fig. S5). This mechanism is most evident over the Sahara, where the high ratio of RX5day to annual precipitation is associated with larger blue water shares (Figs. 1a and S5).

https://doi.org/10.5194/egusphere-2025-5896
Preprint. Discussion started: 4 December 2025

Yet, runoff parameterisation in CMIP6 land-surface schemes emphasise saturation-excess and under-represent infiltration-excess runoff, which may explain why Saharan blue water dominance is more pronounced in observation-based products (Hou et al., 2023) (Fig. S1).

Precipitation-intensity regulated partitioning, the third BGWS feature, emerges in the humid subtropical and tropical regions. Larger blue water shares occur where high mean and intense precipitation (RX5day) keep the upper soil near saturation more often. This yields higher saturation-excess runoff for a given transpiration demand. In contrast, in humid regions where mean and intense precipitation are insufficient to maintain wet upper soils, saturation events are rarer and partitioning shifts toward green water. This asymmetric feature can be observed when comparing the major rainforests (Fig. 1a). While the rainforests of northern South America and central Africa primarily favour green water dominance, the Southeast Asian rainforest demonstrates a contrasting pattern. Transpiration is of similar magnitude across the major rainforests (Fig. 1d). Hence, this BGWS asymmetry is likely due to Southeast Asia receiving more mean and intense precipitation associated with stronger Monsoon rains, and corresponding higher upper soil moisture (Figs. 1b and S4). Assuming broadly similar soil properties across rainforests, more frequent near-saturation in Southeast Asia generates more saturation-excess runoff and larger blue water shares (Fig. 1a,c). Compared with observation-based products, this rainforest asymmetry differs, with the Amazon showing slightly larger blue water shares (Fig. S1).

Similarly, subtropical regions with relatively high mean precipitation and RX5day, such as southern China and southern Japan – both influenced by the East Asian Summer Monsoon – experience higher upper soil moisture and corresponding elevated runoff (Figs. 1b,c and S4). Consequently, these regions exhibit greater partitioning towards blue water flows (Fig. 1a). In contrast, subtropical regions with larger green water shares, such as the Florida Peninsula, mostly exhibit lower mean and intense precipitation with correspondingly drier upper soils and reduced runoff, while transpiration remains at levels comparable to, e.g., southern China (Fig. 1 and S4). This green water dominance may also be influenced by rainfall distribution, as more evenly spread precipitation can sustain higher transpiration throughout the year. Notably, significant ensemble disagreement exists underscoring the challenges ESMs face in accurately representing humid subtropical and tropical hydroecological dynamics (Fiedler et al., 2020; Padrón et al., 2022) (Fig. S6).

3.2 Projected changes in the Blue-Green Water Share

Figure 2a maps the projected BGWS changes (2071-2100 minus 1985-2014) under the regional rivalry scenario (SSP3-7.0), categorising grid cells based on whether they have a positive or negative historical BGWS. The figure highlights either a strengthening or weakening of the existing blue or green water regime, with each of these four trends covering similar proportions of the global land area (Table S3). Notably, a regime shift from blue towards green water is projected in 4% of global land area, while the reverse is simulated in 6.3% (Fig. S7 and Table S4). The balanced distribution of global BGWS trends cancel out opposing changes, yielding no discernible mean trend. However, individual model projections vary considerably, with global mean changes ranging from -2% to +5% (Table S2).

https://doi.org/10.5194/egusphere-2025-5896
Preprint. Discussion started: 4 December 2025

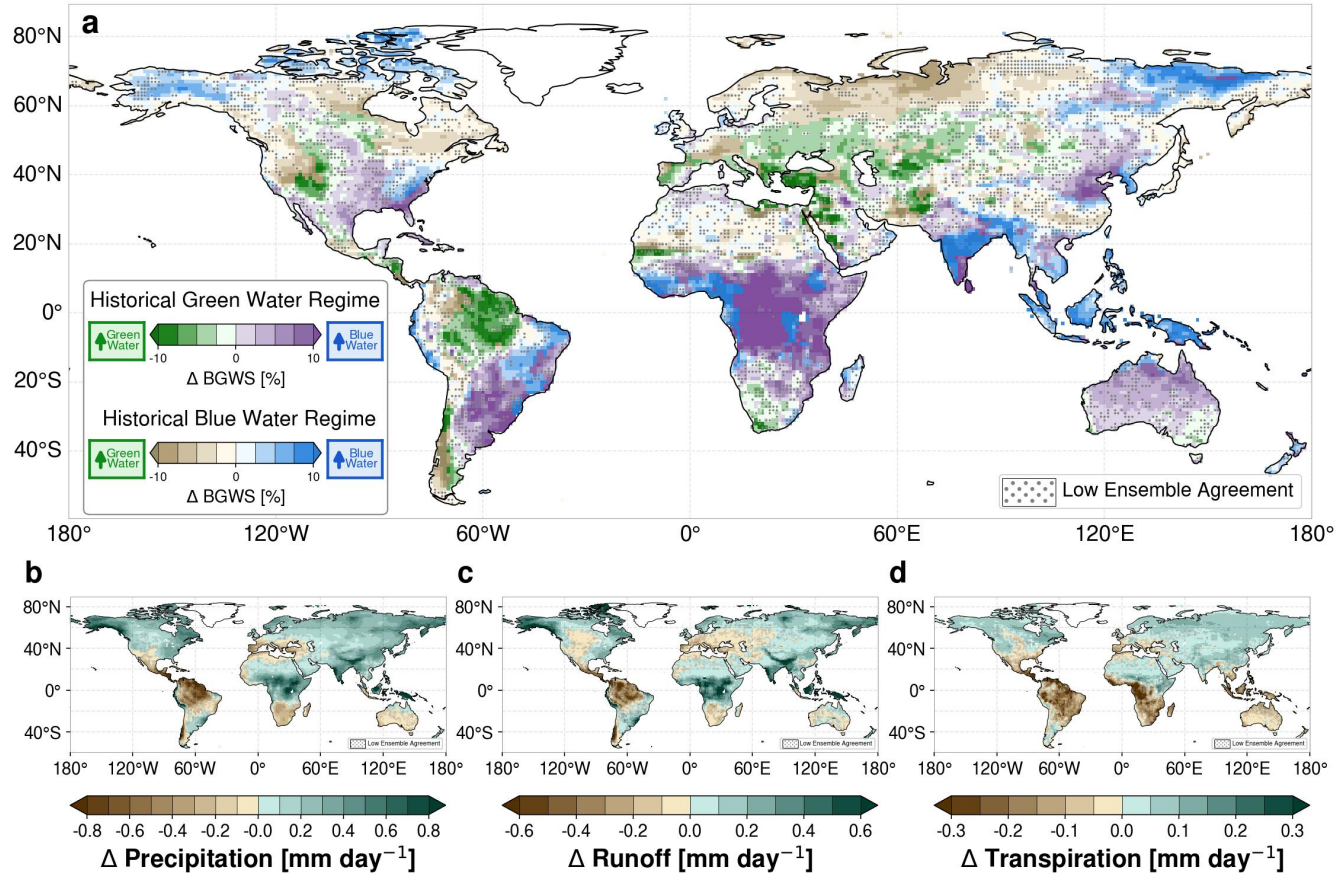

Figure 2. Ensemble mean change (2071–2100 minus 1985–2014) under the SSP3-7.0 scenario based on 11 CMIP6 ESMs. a, Δ Blue-Green Water Share (BGWS) [%], shown separately for grid cells with historically positive (Blue Water Regime; green to purple colours) and negative (Green Water Regime; beige to blue colours) values. Blue and purple colours indicate increasing blue water shares, while green and beige colours indicate increasing green water shares. b, Δ precipitation [mm day^{-1}], c, Δ runoff [mm day^{-1}], and d, Δ transpiration [mm day^{-1}]. Stipplings denote regions of low ensemble agreement where less than 70% of the 11 ensemble members agree on the sign of the change.

In the higher latitudes ($> 60°$N), equal land areas (~ 50 %) experience amplification or weakening of the historical blue water regime (Fig. 2a). Despite ensemble variability, robust blue water share increases are present in, e.g., Alaska, strongly associated with enhanced precipitation (Fig. 2a,b). In contrast, areas with a robust increase in the green water share, e.g., northwestern Eurasia, are strongly linked to expanding leaf area (Fig. S8e). Here, rising transpiration demand exceeds additional precipitation supply, resulting in increasing green water shares (Fig. 2). Although a larger share of precipitation is partitioned towards green water flow, these regions concurrently experience an increase in blue water flow (Fig. 2c; see also Fig. S9 for relative changes). This highlights the function of the BGWS metric, which emphasizes changes in water partitioning rather than absolute shifts in water availability (see Sect. 3.4).

https://doi.org/10.5194/egusphere-2025-5896
Preprint. Discussion started: 4 December 2025

Unlike the balanced BGWS response in higher latitudes, 73% of mid-latitudes experience green water share increases, associated with substantial vegetation growth (Fig. S8e). In some regions, e.g., central Europe, this green water gain coincides with runoff loss (Fig. 2c). Most mid-latitude regions with increasing blue water shares also show rising runoff (e.g., the mid-latitude East Asian monsoon belt; Fig. 2a). However, in parts of the historically water-limited West North Central U.S. and the Canadian Prairies (purple in Fig. 2a), blue water shares increase because transpiration decreases more than runoff (Fig. 2c,d). A similar pattern of blue water share increases occurs in subtropical patches in e.g. Mexico and Australia, where the relative decline in transpiration exceeds runoff loss (Fig. 2c,d). This contrasts with observed CO_2-driven blue water losses where greening increased evapotranspiration and reduced streamflow (Australia's sub-humid/semi-arid basins (Ukkola et al., 2016)) and with vegetation-driven runoff declines in the American West (Mankin et al., 2017, 2019). Over Australia, however, our result is consistent with ESM projections of increased runoff partitioning under CO_2 forcing (Mankin et al., 2019). While the LAI primarily increases in response to CO_2 fertilisation, transpiration decreases as higher WUE offsets rising water demands (Figs. 2d and S8). Nonetheless, large areas are projected to experience blue water loss, as receiving a larger share of precipitation does not offset the overall decline in blue water (Fig. 2c). The responses to elevated CO_2 effects on hydrological processes should, however, be interpreted with caution given the considerable variability in CMIP6 models (Wei et al., 2024). Moreover, plants' water savings due to increased WUE do not always prevail. Southern Europe, for instance, is characterised by a greater reduction in runoff compared to transpiration, hence, experiencing a green water share increase (Fig. 2). Overall, whether dry regions will experience a blue or green water share increase, depends largely on the interplay between rising vegetational water demand and WUE-related transpiration limitations. In the subtropics, 60% of the land area is projected to experience a greater blue water share, dominated by already wet regions, e.g., in Eastern Asia. Additionally, vegetation responses influence subtropical BGWS trends, though structural uncertainties remain in how models represent vegetation's response to rising CO_2 and corresponding water cycle impacts (Yang et al., 2021; Forzieri et al., 2020; Yang et al., 2023).

The BGWS response in humid subtropical and tropical regions remains highly sensitive to precipitation patterns and extremes. The major rainforests exhibit an asymmetric response, with only the Amazon rainforest showing an increasing green water share. In contrast, the Central African and Southeast Asian rainforests are projected to shift towards a greater blue water share. This divergence aligns with precipitation and runoff trends – both decreasing over the Amazon but increasing in the other two regions, while transpiration declines across all three (Fig. 2b-c). In other tropical regions with a positive historical BGWS, e.g., large parts of India, future trends are generally positive, driven by increased wetting and scattered decreases in transpiration (Fig. 2). Overall, a majority (73%) of tropical land is projected to experience greater blue water shares, highlighting vegetation's response to rising CO_2 as a key factor amid contrasting trends in transpiration.

3.3 Extreme precipitation strongly impacts global BGWS change

Precipitation partitioning changes between blue and green water flows are driven by various climatic and non-climatic factors. Our analysis of historical characteristics and projected changes in BGWS presents a unique opportunity to uncover key controlling factors behind shifts in blue-green water partitioning. We hypothesize that these shifts originate from alterations in mean and extreme precipitation, changes in atmospheric and soil-moisture deficits, and vegetation responses. To quantify

https://doi.org/10.5194/egusphere-2025-5896
Preprint. Discussion started: 4 December 2025

their impacts, we performed multiple linear regression (MLR) analyses for each BGWS regime (Methods). Both MLR models exhibit moderate predictive power (Fig. 3a,b). However, consistent variable importance rankings across training and testing datasets suggest robust and interpretable results (Breiman, 2001) (Fig. S10). We validate our approach by comparing MLR importance rankings with those from random forest models. The similarity in results between these two independent methods supports the robustness of our findings (Fig. S11).

Our results in Fig. 3a,b demonstrate that BGWS alterations in both regimes are most sensitive to extreme five-day precipitation changes. RX5day is projected to increase across all ensemble members, consistent with theoretical expectations that warming-driven increases in atmospheric moisture intensify precipitation extremes (Trenberth, 2011; Donat et al., 2016; Tabari, 2020) (Fig. 3c,d). Its positive regression coefficient indicates that higher RX5day contributes to larger blue water shares. This relationship arises as high precipitation amounts over short periods can quickly saturate soils, triggering saturation-excess runoff in CMIP6 land-surface schemes. The RX5day effect would likely be even larger in models that also represent infiltration-excess runoff, which only a few schemes currently include (Hou et al., 2023). Additionally, stormier conditions typically increase cloud cover, which reduces incoming shortwave radiation and thereby transpiration. This energy constraint may further reinforce the positive association between higher RX5day and larger blue water shares (Wang et al., 2023).

Our findings emphasize two key points. First, while mean precipitation might regionally decrease, the intensification of intense rainfall (RX5day) induces the mean blue water share to rise. This suggests an intensification of runoff events even when the average runoff is decreasing. Although more precipitation is thus periodically partitioned towards blue water, questions remain about its accessibility under climate change, including potential adverse flood impacts and opportunities for replenishing water storages.

Second, in regions with enhanced mean precipitation, increases in RX5day augment the blue water share. In these cases, soils may become saturated more frequently linked to increasing baseline rainfall (Fig. S8c). Consequently, subsequent extreme precipitation events are more likely to trigger flooding, further highlighting the challenges that larger blue water shares pose for water management. The dependence of RX5day magnitudes on baseline precipitation stresses the importance of also considering average precipitation change (Fig. 3a,b). This effect may particularly emerge in the blue water regime, where average precipitation is projected to increase in over 89% of the area, with a mean increase of 0.24 $\mathrm{mm\,day^{-1}}$ ($\sim$8 %) (Fig. 3c).

Besides precipitation intensification, changes in LAI show a strong relationship with BGWS trends. Global greening is evident in the ensemble mean, with LAI increases that are nearly twice as large in the blue water regime (Fig. 3c,d). Particularly blue water-dominated higher and mid-latitudes experience extensive vegetation growth due to global warming, where energy and temperature limitation is the primary controlling factor. Besides, CO_2 fertilisation and scenario-dependent land-use changes further impact LAI (Hurtt et al., 2020; Zhao et al., 2020). The potential expansion in vegetation increases transpiration water demand, contributing to a larger green water share, as reflected by the strong negative regression coefficient. In addition, greater LAI elevates canopy interception losses, reducing throughfall and runoff and potentially reinforcing green-ward shifts. In the green water regime, LAI changes have a similar positive effect on the green water share, but their importance to BGWS change is lower (Fig. 3b).

https://doi.org/10.5194/egusphere-2025-5896
Preprint. Discussion started: 4 December 2025

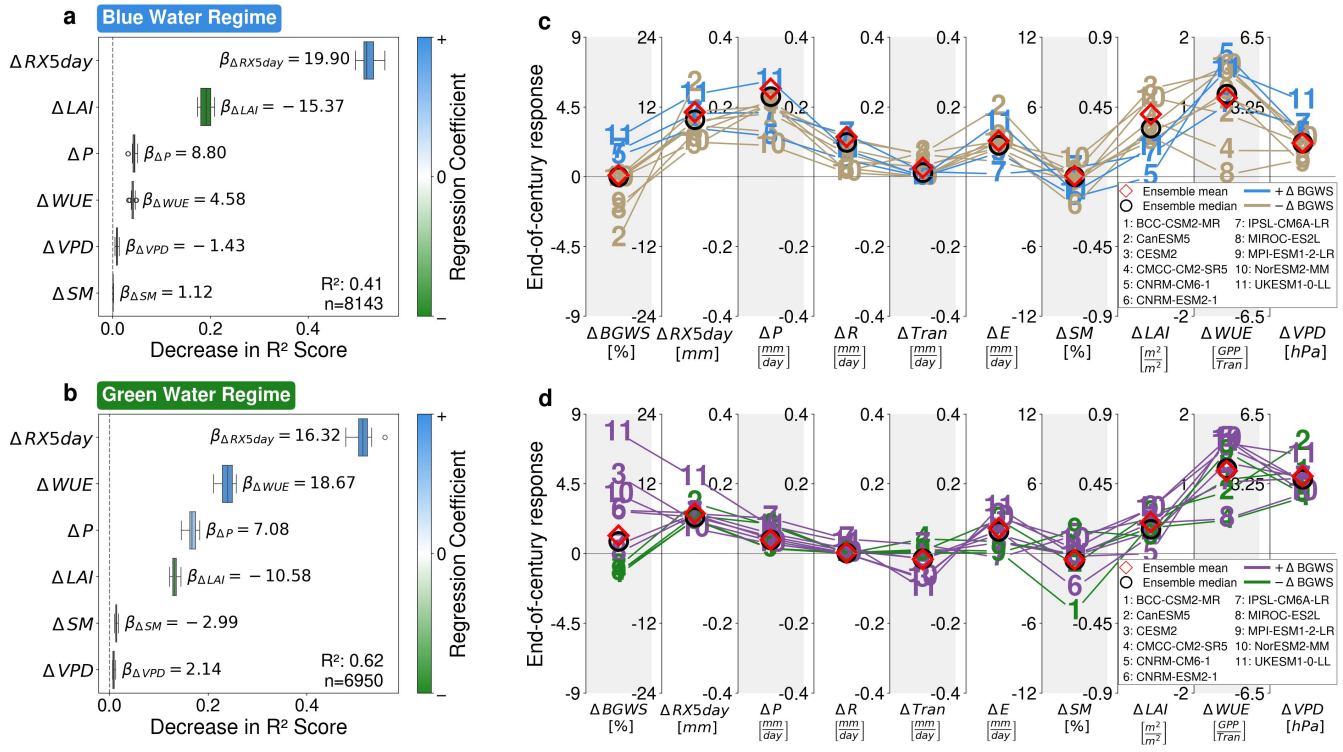

Figure 3. Global mean variable changes (2071–2100 minus 1985–2014) under the SSP3-7.0 scenario and importance ranks across the blue and green water regimes based on 11 CMIP6 ESMs. a, b, Variable importance plots present the decrease in accuracy score of selected predictors based on the permutation importance analysis for the testing dataset of the a, blue water regime and b, green water regime. Variable importance rankings correspond to each predictor's contribution in explaining Blue–Green Water Share (BGWS) changes (2071–2100 minus 1985–2014) under the SSP3-7.0 scenario. The colour of the boxes indicates the regression coefficient β, with blue representing a positive β (positive relationship with blue water share) and green a negative β (positive relationship with green water share). Here, β represents the strength and direction of the relationship between each predictor and the BGWS change. Model performance on the testing dataset (R^2) and the number of grid cells considered in this analysis (n) are indicated. c, d, Parallel-coordinates plot presenting mean end-of-century responses of BGWS (ΔBGWS), annual maximum consecutive five-day precipitation (ΔRX5day), precipitation (ΔP), runoff (ΔR), transpiration (ΔTran), evaporation (ΔE), soil moisture (ΔSM), leaf area index (ΔLAI), water-use efficiency (ΔWUE), and vapour pressure deficit (ΔVPD) in the c, blue water regime and d, green water regime. Numbers indicate results for each of the eleven CMIP6 models and help identify outliers. Red diamonds indicate the ensemble mean, black circles the ensemble median response. Model and line colours in c (blue) and d (purple) indicate models with a positive BGWS change, whereas beige in c and green in d represent models with a negative BGWS change.

WUE is increasing in both regimes, likely due to rising CO_2 levels that affect stomatal conductance and GPP. The increase is smaller in blue water-dominated regions (Fig. 3c,d), which might be due to sufficient water availability in most blue water areas and plant-type-specific responses (Gentine et al., 2019). Yet, the latter processes are insufficiently captured in ESMs as plant functional types are limited in number and oversimplify ecological dynamics (Anderegg et al., 2022). WUE effects on

https://doi.org/10.5194/egusphere-2025-5896
Preprint. Discussion started: 4 December 2025

BGWS trends are particularly strong in the green water regime (Fig. 3b). Here, the ensemble mean shows a decrease in mean transpiration, despite expanding vegetation (Fig. 3d). The suppressing effect of rising WUE on green water flow leads to an increase in the blue water share (Fig. 3b), consistent with the "plants-turn-on-the-tap" mechanism (Idso and Brazel, 1984). Consequently, WUE changes play a key role in blue water share increases within the green water regime (i.e., 30.9% of global land area with blue water share increases within the green water regime) and potentially drive the green-to-blue regime shift observed in 6.3% of the global land area (Tables S3 and S4).

3.4 Management implications of future BGWS trends

The BGWS metric is a process rather than a quantity indicator. It characterises how an incremental unit of precipitation (e.g., the next millimetre of rain) is partitioned between runoff (blue water) and plant use via transpiration (green water), not how large those fluxes are in absolute terms. In this sense, BGWS addresses the question "where does the next unit of rain tend to go?" rather than "how much water is there overall?". This distinction matters for impacts that depend on hydrological sensitivity and timing (Nijssen et al., 2001), such as runoff responsiveness (flashiness), baseflow sustainment, soil-moisture buffering, and canopy evaporative cooling, affecting both ecosystems and human water management, even when absolute amounts of precipitation, runoff, or transpiration rise or fall. It shifts the focus from one on absolute change, to one in which we try to understand controlling factors and enables another level of model evaluation that centres on comparing these controlling factors rather than just focusing on matching historical observations (Wagener et al., 2022). Although our analysis is flow-based and excludes storage terms, persistent BGWS shifts signal sustained pressure on blue water stores (e.g., rivers, reservoirs, groundwater) versus green water stores (root-zone moisture).

BGWS changes become most meaningful for management when interpreted jointly with absolute hydroecological changes rather than analysing partitioning shifts or absolute changes (e.g., RX5day) in isolation. This joint interpretation provides a more complete picture of blue and green water processes and their implications. For water management, combining BGWS changes with absolute changes in runoff yields decision-relevant insights (Fig. 4a; conceptual synthesis in Fig. 5). Where BGWS and runoff changes are both positive, managers should anticipate greater potential for flood pressure, which enhances channel erosion and nutrient flushing (e.g., southern Asia); where ΔBGWS is positive but runoff change is negative, absolute runoff shrinks yet vegetation water use declines even more strongly (e.g., western Mediterranean). Thus, the relative contribution of runoff pathways per unit precipitation increases, thereby raising the potential for intense runoff generation during extreme precipitation events. This aligns with catchment-scale evidence that rising precipitation intensity shifts precipitation partitioning toward fast runoff, erodes green water storage, and threatens reservoir reliability (Eekhout et al., 2018). Conversely, negative ΔBGWS with positive runoff change suggests more total runoff but a smaller fraction per event, potentially improving baseflow support if soil moisture increases (e.g., Eastern Canada); when both ΔBGWS and runoff changes are negative, shrinking blue water volumes and shares indicate water-scarcity and ecological-flow risks that call for demand management, soil-moisture conservation and increased storage (e.g., Amazon rainforest). Comparable patterns are seen during European droughts, where blue water declines outpace green water responses, tightening low-flows even when vegetation maintains transpiration (Orth and Destouni, 2018).

https://doi.org/10.5194/egusphere-2025-5896
Preprint. Discussion started: 4 December 2025

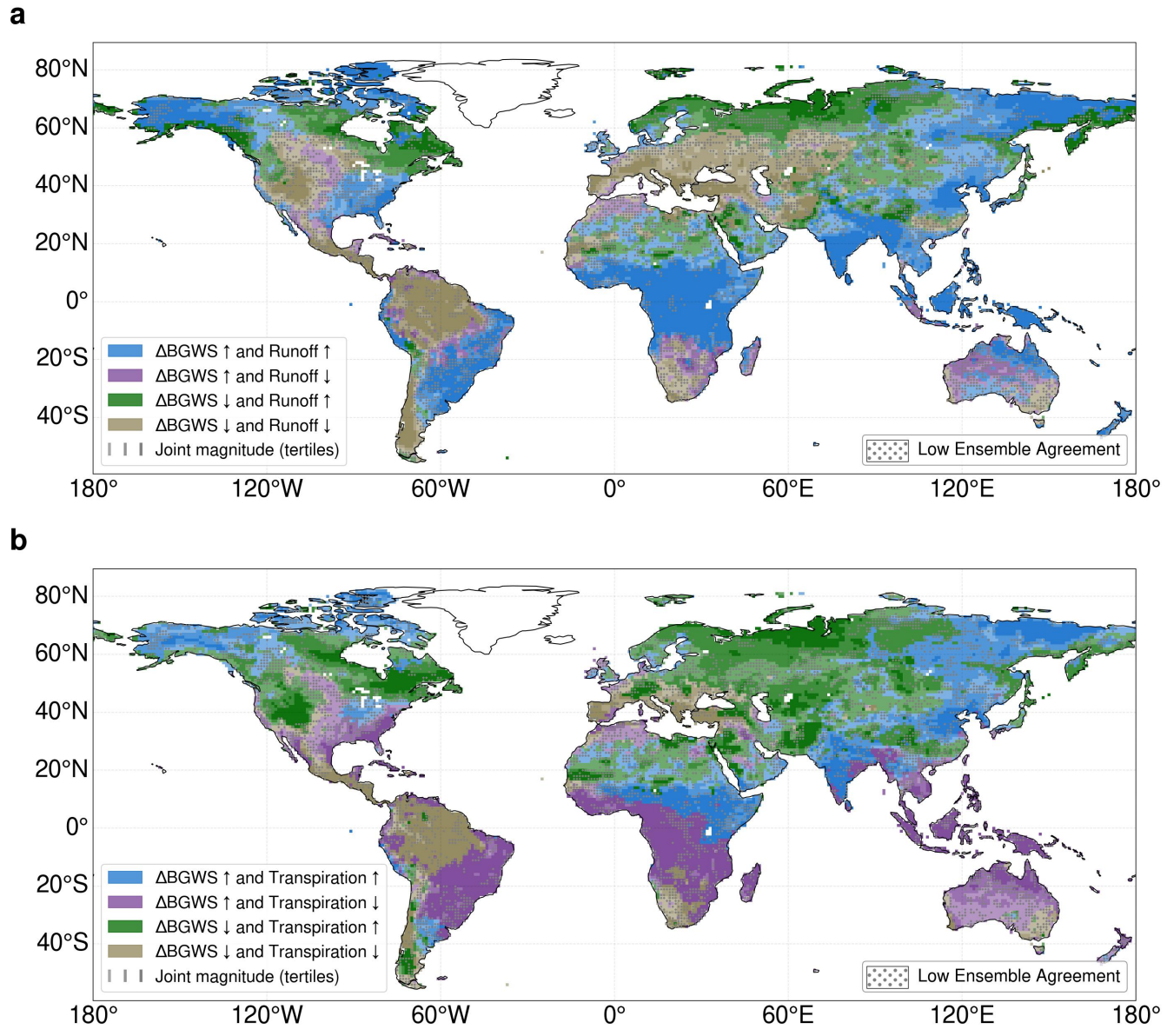

Figure 4. Joint ensemble-mean change (2071–2100 minus 1985–2014) of the Blue–Green Water Share (BGWS) with blue and green water flows under the SSP3-7.0 scenario, based on 11 CMIP6 ESMs. a, Relationship between simulated changes in BGWS and runoff. b, Relationship between simulated changes in BGWS and transpiration. Colours encode the quadrant of joint change (blue = ΔBGWS ↑ & flow ↑, violet = ΔBGWS ↑ & flow ↓, green = ΔBGWS ↓ & flow ↑, brown = ΔBGWS ↓ & flow ↓). Lightness indicates the relative magnitude of change (tertiles from the joint distribution). Grey stippling marks grid cells with low ensemble agreement on the sign of change (<70 % of models).

https://doi.org/10.5194/egusphere-2025-5896
Preprint. Discussion started: 4 December 2025

For land-management, interpreting BGWS jointly with absolute changes in transpiration provides eco-physiological insight (Fig. 4b; conceptual synthesis in Fig. 5). Where BGWS and transpiration increase, landscapes become more runoff-dominated while plant water use rises, signalling higher atmospheric/phenological demand and reliance on stored water (e.g., Horn of Africa); where BGWS increases but transpiration decreases, partitioning shifts toward runoff as vegetation down-regulates (e.g., C. Australia). The latter response reduces evaporative cooling and elevates heat-risk (He et al., 2022). Conversely, BGWS decreases with transpiration increases indicate greater green water allocation and stronger latent cooling, supporting vegetation productivity and microclimate buffering, but they also signal faster soil-moisture depletion and rising irrigation demand when precipitation decreases (e.g., western North America); when both BGWS and transpiration decrease, relative allocation to green water rises despite lower plant water use, flagging weaker evaporative cooling and habitat stress (e.g., Amazon rainforest).

	↑ Runoff	↓ Runoff	↑ Transpiration	↓ Transpiration
↑ BGWS	**Implications:** • More runoff-oriented partitioning • Greater potential for flood pressure, channel erosion and nutrient flushing **Example Regions:** Central-Africa, S.E. South-America, S. Asia	**Implications:** • Decreasing total runoff but reduced vegetative buffering • Greater low-flow stress • Increased hydrological sensitivity to intense rainfall (conditional flood risk) **Example Regions:** C. Australia, E. Southern-Africa, W. Mediterranean	**Implications:** • More runoff-oriented partitioning while plant water use rises • Higher atmospheric/phenological water demand • Greater reliance on stored water during dry periods **Example Regions:** E. Siberia, Horn of Africa, S. Asia	**Implications:** • Vegetation down-regulation shifts partitioning toward runoff • Reduced evaporative cooling and weakened microclimate buffering • Elevated heat-stress risk **Example Regions:** S.E. Asia, C. Australia, Central-Africa
↓ BGWS	**Implications:** • Greater total runoff but smaller fraction per event • Improved baseflow support if soil moisture increases **Example Regions:** Eastern Canada, W. Siberia, N. Europe	**Implications:** • Increased risk of blue water scarcity & ecological-flow stress • Need for demand management, soil-moisture conservation, and additional storage **Example Regions:** Amazon rainforest, W. & C. Europe, W. North-America	**Implications:** • Increasing green-water share and latent cooling • Enhanced plant productivity and microclimate buffering • Higher irrigation demand under drying **Example Regions:** W.C. Asia, W. Siberia, W. North America	**Implications:** • Green water share rises despite lower plant use • Weaker evaporative cooling and habitat stress **Example Regions:** Amazon rainforest, E. Mediterranean, S.E. Australia

Figure 5. Conceptual classification matrix illustrating the implications of joint projected changes (2071–2100 minus 1985–2014) in the Blue-Green Water Share (BGWS) and absolute runoff and transpiration. The matrix summarises the dominant hydrological and ecological responses associated with the direction of joint ensemble-mean changes in BGWS and absolute flows under SSP3-7.0, based on 11 CMIP6 ESMs. Coloured labels correspond to the four quadrants of joint change (blue = ΔBGWS ↑ & flow ↑; violet = ΔBGWS ↑ & flow ↓; green = ΔBGWS ↓ & flow ↑; brown = ΔBGWS ↓ & flow ↓).

In communicating results, uncertainty is decision-relevant and should be made explicit. In blue water regimes, spatial means indicate both larger responses and larger inter-model spread in hydrological variables and vegetation metrics, whereas in green water regimes the mean hydrological response is more certain but the spread in transpiration remains comparably large

https://doi.org/10.5194/egusphere-2025-5896
Preprint. Discussion started: 4 December 2025

(Fig. 3c,d). Our maps further show that sizeable areas do not reach ≥ 70 % ensemble agreement (i.e. fewer than 8 of 11 models), signalling sign-uncertain change at the grid-cell scale (Figs. 2, 4 and S8). Water and land management should therefore distinguish sign-robust patterns, which justify no-regrets measures consistent with the implied risk pathway, from magnitude- or sign-uncertain patterns, which call for adaptive pathways, flexible design ranges, and enhanced monitoring. Given the additional baseline biases relative to observation-based products (Figs. S1, S2 and S3), a regionalised and observationally constrained analysis of ΔBGWS and co-varying hydroecological responses could yield actionable, sector-specific insights for water allocation, flood protection, irrigation demand, environmental flows, and heat mitigation.

4 Discussion and conclusion

The introduction of the BGWS brings several advances in quantifying and understanding precipitation partitioning between blue and green water, and its combination with absolute changes in hydroecological variables yields impact-relevant insights.

Our finding that extreme precipitation changes have the largest impact on partitioning shifts aligns with studies showing strong effects of rainfall extremes on runoff ratios and catchment retention (Yang et al., 2018; Scheff et al., 2022). We extend this insight from retention and runoff volumes to an explicit partitioning metric that includes transpiration. This links precipitation intensity and plant physiology to how precipitation is partitioned between channel flow and plant use. Separating historical blue and green regimes clarifies offsetting effects that can mask net global signals in runoff ratios. We also concur with Yang et al. (Yang et al., 2018) that explicitly quantifying intra-annual hydroclimate variability would enhance understanding in highly seasonal climates. We extend this recommendation to precipitation-partitioning dynamics.

Relative to the blue water trade-off (BWT) metric used by Mankin et al. (Mankin et al., 2018, 2019), the BGWS contrasts runoff directly with transpiration, excluding interception or storage, and reports it as a normalised share of precipitation. Thus, interception-driven canopy effects are not represented explicitly by the BGWS. For assessing green water, however, transpiration as a direct ESM output is beneficial and more readily translated to land-management perspectives as the immediate indicator of plant water use. In contrast to Mankin et al. (Mankin et al., 2018), who found that increased blue water partitioning arises primarily from mean-precipitation increases reinforced by extremes, we show that extreme five-day precipitation is the dominant driver of partitioning change. This is apparent across both historical regimes and independent of baseline precipitation. Considering BGWS alongside absolute changes in runoff and transpiration provides a compact interpretation that moves beyond quantifying partitioning shifts and connects them to potential impacts on communities and ecosystems.

Together, these advances position BGWS as a simple, interpretable metric that isolates the runoff–transpiration pathway, elevates RX5day as the leading global driver, identifies LAI and WUE as secondary regime-dependent controls, and, when paired with absolute runoff and transpiration changes, translates partitioning shifts into decision-relevant guidance. BGWS complements, rather than replaces, canopy-focused trade-off and retention metrics.

Nonetheless, uncertainties and biases in ESM studies remain since BGWS dynamics depend on the representation of hydroclimatic and biogeochemical processes (Clark et al., 2015; Gentine et al., 2019; Zheng et al., 2019; Padrón et al., 2022; Yang et al., 2023; Gier et al., 2024). Despite these uncertainties, particularly in the land-surface components and

https://doi.org/10.5194/egusphere-2025-5896
Preprint. Discussion started: 4 December 2025

their assumptions regarding plant responses to elevated CO_2 , robust signals of BGWS shifts emerge. Yet, advancing both observational data and ESMs appears vital to improve the reliability of future projections on terrestrial freshwater availability. Coupling these advancements with process-based ESM evaluations will deepen insights into blue-green water partitioning and vegetation-climate feedbacks, paving the way for more robust and actionable climate information, especially in understudied, high-impact regions (Stein et al., 2024).

Code and data availability. The CMIP6 datasets used in this study were accessed through the Deutsche Klimarechenzentrum (DKRZ) CMIP Data Pool and the Pangeo CMIP6 Catalog (last access: 20 December 2024). The DKRZ CMIP Data Pool (available at https://cmip-data-pool.dkrz.de) is restricted to registered users with a valid DKRZ account. The datasets are also publicly available through the Earth System Grid Federation (https://aims2.llnl.gov) portal and the Copernicus Climate Data Store (CDS) (https://cds.climate.copernicus.eu). The Pangeo CMIP6 Catalog (available at https://storage.googleapis.com/cmip6 /pangeo-cmip6.json) is publicly accessible. The GPCC monthly product is available for download from DWD Open Data: https://opendata.dwd.de/climate_environment /GPCC/html/fulldata-monthly_v2022_doi_download.html (last access: 10 January 2025). The G-RUN dataset is publicly available at Figshare: https://figshare.com/articles/dataset/G-RUN_ENSEMBLE/12794075 (last access: 10 January 2025). The GLEAM dataset is available via SFTP (Secure File Transfer Protocol) and requires user registration for access. Credentials can be requested at GLEAM website: https://www.gleam.eu (last access: 10 January 2025). ERA5 land data is publicly available through the Copernicus CDS (last access: 10 January 2025). All code to reproduce this analysis is publicly available on GitHub at: https://github.com/simonheselschwerdt/bgws_analysis.

Author contributions. S.P.H. and P.G. conceived the study and designed the analysis. S.P.H. conducted the analysis and led the writing of the manuscript. All authors discussed the methods and results and contributed to writing and edited the manuscript.

Competing interests. Some authors are members of the editorial board of Earth System Dynamics.

Acknowledgements. This study is financially supported by the Helmholtz Association Initiative and Networking Fund (IVF). We acknowledge the World Climate Research Programme's Working Group on Coupled Modelling, which is responsible for CMIP, and we thank the climate modelling groups for producing and making available their model output. This work used resources of the Deutsches Klimarechenzentrum (DKRZ, https://www.dkrz.de) granted by its Scientific Steering Committee (WLA) under project ID ch0636. S.P.H. and P.G. also thank Peter Hoffmann for internally reviewing our paper draft. T.W. acknowledges support from the Alexander von Humboldt Foundation in the framework of the Alexander von Humboldt Professorship endowed by the German Federal Ministry of Education and Research (BMBF).

https://doi.org/10.5194/egusphere-2025-5896
Preprint. Discussion started: 4 December 2025

References

Anderegg, L. D. L., Griffith, D. M., Cavender-Bares, J., Riley, W. J., Berry, J. A., Dawson, T. E., and Still, C. J.: Representing plant diversity in land models: An evolutionary approach to make "Functional Types" more functional, Global Change Biology, 28, 2541–2554, https://doi.org/10.1111/gcb.16040, 2022.

Barnett, T. P., Adam, J. C., and Lettenmaier, D. P.: Potential impacts of a warming climate on water availability in snow-dominated regions, Nature, 438, 303–309, https://doi.org/10.1038/nature04141, 2005.

Betts, R. A., Cox, P. M., Collins, M., Harris, P. P., Huntingford, C., and Jones, C. D.: The role of ecosystem-atmosphere interactions in simulated Amazonian precipitation decrease and forest dieback under global climate warming, Theoretical and Applied Climatology, 78, 157–175, https://doi.org/10.1007/s00704-004-0050-y, 2004.

Betts, R. A., Boucher, O., Collins, M., Cox, P. M., Falloon, P. D., Gedney, N., Hemming, D. L., Huntingford, C., Jones, C. D., Sexton, D. M. H., and Webb, M. J.: Projected increase in continental runoff due to plant responses to increasing carbon dioxide, Nature, 448, 1037–1041, https://doi.org/10.1038/nature06045, 2007.

Boucher, O., Servonnat, J., Albright, A. L., Aumont, O., Balkanski, Y., Bastrikov, V., Bekki, S., Bonnet, R., Bony, S., Bopp, L., Braconnot, P., Brockmann, P., Cadule, P., Caubel, A., Cheruy, F., Codron, F., Cozic, A., Cugnet, D., D'Andrea, F., Davini, P., de Lavergne, C., Denvil, S., Deshayes, J., Devilliers, M., Ducharne, A., Dufresne, J.-L., Dupont, E., Éthé, C., Fairhead, L., Falletti, L., Flavoni, S., Foujols, M.-A., Gardoll, S., Gastineau, G., Ghattas, J., Grandpeix, J.-Y., Guenet, B., Guez, Lionel, E., Guilyardi, E., Guimberteau, M., Hauglustaine, D., Hourdin, F., Idelkadi, A., Joussaume, S., Kageyama, M., Khodri, M., Krinner, G., Lebas, N., Levavasseur, G., Lévy, C., Li, L., Lott, F., Lurton, T., Luyssaert, S., Madec, G., Madeleine, J.-B., Maignan, F., Marchand, M., Marti, O., Mellul, L., Meurdesoif, Y., Mignot, J., Musat, I., Ottlé, C., Peylin, P., Planton, Y., Polcher, J., Rio, C., Rochetin, N., Rousset, C., Sepulchre, P., Sima, A., Swingedouw, D., Thiéblemont, R., Traore, A. K., Vancoppenolle, M., Vial, J., Vialard, J., Viovy, N., and Vuichard, N.: Presentation and Evaluation of the IPSL-CM6A-LR Climate Model, Journal of Advances in Modeling Earth Systems, 12, e2019MS002 010, https://doi.org/10.1029/2019MS002010, 2020.

Breiman, L.: Random Forests, Machine Learning, 45, 5–32, https://doi.org/10.1023/A:1010933404324, 2001.

Buck, A. L.: New Equations for Computing Vapor Pressure and Enhancement Factor, Journal of Applied Meteorology and Climatology, 20, 1527–1532, https://doi.org/10.1175/1520-0450(1981)020<1527:NEFCVP>2.0.CO;2, 1981.

Budyko, M. I.: Climate and Life, Academic Press, New York, 1974.

Cherchi, A., Fogli, P. G., Lovato, T., Peano, D., Iovino, D., Gualdi, S., Masina, S., Scoccimarro, E., Materia, S., Bellucci, A., and Navarra, A.: Global Mean Climate and Main Patterns of Variability in the CMCC-CM2 Coupled Model, Journal of Advances in Modeling Earth Systems, 11, 185–209, https://doi.org/10.1029/2018MS001369, 2019.

Clark, M. P., Fan, Y., Lawrence, D. M., Adam, J. C., Bolster, D., Gochis, D. J., Hooper, R. P., Kumar, M., Leung, L. R., Mackay, D. S., Maxwell, R. M., Shen, C., Swenson, S. C., and Zeng, X.: Improving the representation of hydrologic processes in Earth System Models, Water Resources Research, 51, 5929–5956, https://doi.org/10.1002/2015WR017096, 2015.

Danabasoglu, G., Lamarque, J.-F., Bacmeister, J., Bailey, D. A., DuVivier, A. K., Edwards, J., Emmons, L. K., Fasullo, J., Garcia, R., Gettelman, A., Hannay, C., Holland, M. M., Large, W. G., Lauritzen, P. H., Lawrence, D. M., Lenaerts, J. T. M., Lindsay, K., Lipscomb, W. H., Mills, M. J., Neale, R., Oleson, K. W., Otto-Bliesner, B., Phillips, A. S., Sacks, W., Tilmes, S., van Kampenhout, L., Vertenstein, M., Bertini, A., Dennis, J., Deser, C., Fischer, C., Fox-Kemper, B., Kay, J. E., Kinnison, D., Kushner, P. J., Larson, V. E., Long, M. C., Mickelson, S., Moore, J. K., Nienhouse, E., Polvani, L., Rasch, P. J., and Strand, W. G.: The Community Earth System Model Version 2 (CESM2), Journal of Advances in Modeling Earth Systems, 12, e2019MS001 916, https://doi.org/10.1029/2019MS001916, 2020.

https://doi.org/10.5194/egusphere-2025-5896
Preprint. Discussion started: 4 December 2025

Donat, M. G., Lowry, A. L., Alexander, L. V., O'Gorman, P. A., and Maher, N.: More extreme precipitation in the world's dry and wet regions, Nature Climate Change, 6, 508–513, https://doi.org/10.1038/nclimate2941, 2016.

Dunne, T. and Black, R. D.: An Experimental Investigation of Runoff Production in Permeable Soils, Water Resources Research, 6, 478–490, https://doi.org/10.1029/WR006i002p00478, 1970.

Dutta, R. and Markonis, Y.: Does ERA5-land capture the changes in the terrestrial hydrological cycle across the globe?, Environmental Research Letters, 19, 024 054, https://doi.org/10.1088/1748-9326/ad1d3a, 2024.

Eekhout, J. P. C., Hunink, J. E., Terink, W., and de Vente, J.: Why increased extreme precipitation under climate change negatively affects water security, Hydrology and Earth System Sciences, 22, 5935–5946, https://doi.org/10.5194/hess-22-5935-2018, 2018.

Eyring, V., Bony, S., Meehl, G. A., Senior, C. A., Stevens, B., Stouffer, R. J., and Taylor, K. E.: Overview of the Coupled Model Intercomparison Project Phase 6 (CMIP6) experimental design and organization, Geoscientific Model Development, 9, 1937–1958, https://doi.org/10.5194/gmd-9-1937-2016, 2016.

Falkenmark, M.: Land–water linkages: a synopsis, in: Land and Water Integration and River Basin Management, Proceedings of the FAO Workshop, Rome, 31 January–2 February 1993, pp. 15–17, FAO, Rome, https://www.fao.org/4/v5400e/v5400e00.htm, 1995.

Falkenmark, M.: Growing water scarcity in agriculture: future challenge to global water security, Philosophical Transactions of the Royal Society A: Mathematical, Physical and Engineering Sciences, 371, 20120 410, https://doi.org/10.1098/rsta.2012.0410, 2013.

Falkenmark, M. and Rockström, J.: The New Blue and Green Water Paradigm: Breaking New Ground for Water Resources Planning and Management, Journal of Water Resources Planning and Management, 132, 129–132, https://doi.org/10.1061/(ASCE)0733-9496(2006)132:3(129), 2006.

Falkenmark, M. and Rockström, J.: Building Water Resilience in the Face of Global Change: From a Blue-Only to a Green-Blue Water Approach to Land-Water Management, Journal of Water Resources Planning and Management, 136, 606–610, https://doi.org/10.1061/(ASCE)WR.1943-5452.0000118, 2010.

Falkenmark, M., Wang-Erlandsson, L., and Rockström, J.: Understanding of water resilience in the Anthropocene, Journal of Hydrology X, 2, 100 009, https://doi.org/10.1016/j.hydroa.2018.100009, 2019.

Fiedler, S., Crueger, T., D'Agostino, R., Peters, K., Becker, T., Leutwyler, D., Paccini, L., Burdanowitz, J., Buehler, S. A., Cortes, A. U., Dauhut, T., Dommenget, D., Fraedrich, K., Jungandreas, L., Maher, N., Naumann, A. K., Rugenstein, M., Sakradzija, M., Schmidt, H., Sielmann, F., Stephan, C., Timmreck, C., Zhu, X., and Stevens, B.: Simulated Tropical Precipitation Assessed across Three Major Phases of the Coupled Model Intercomparison Project (CMIP), Monthly Weather Review, 148, 3653–3680, https://doi.org/10.1175/MWR-D-19-0404.1, 2020.

Forzieri, G., Miralles, D. G., Ciais, P., Alkama, R., Ryu, Y., Duveiller, G., Zhang, K., Robertson, E., Kautz, M., Martens, B., Jiang, C., Arneth, A., Georgievski, G., Li, W., Ceccherini, G., Anthoni, P., Lawrence, P., Wiltshire, A., Pongratz, J., Piao, S., Sitch, S., Goll, D. S., Arora, V. K., Lienert, S., Lombardozzi, D., Kato, E., Nabel, J. E. M. S., Tian, H., Friedlingstein, P., and Cescatti, A.: Increased control of vegetation on global terrestrial energy fluxes, Nature Climate Change, 10, 356–362, https://doi.org/10.1038/s41558-020-0717-0, 2020.

Fowler, M. D., Kooperman, G. J., Randerson, J. T., and Pritchard, M. S.: The effect of plant physiological responses to rising CO2 on global streamflow, Nature Climate Change, 9, 873–879, https://doi.org/10.1038/s41558-019-0602-x, 2019.

Friedman, J. H., Hastie, T., and Tibshirani, R.: Regularization Paths for Generalized Linear Models via Coordinate Descent, Journal of Statistical Software, 33, 1–22, https://doi.org/10.18637/jss.v033.i01, 2010.

Fujimori, S., Hasegawa, T., Masui, T., Takahashi, K., Herran, D. S., Dai, H., Hijioka, Y., and Kainuma, M.: SSP3: AIM implementation of Shared Socioeconomic Pathways, Global Environmental Change, 42, 268–283, https://doi.org/10.1016/j.gloenvcha.2016.06.009, 2017.

https://doi.org/10.5194/egusphere-2025-5896
Preprint. Discussion started: 4 December 2025

Gedney, N., Huntingford, C., Weedon, G. P., Bellouin, N., Boucher, O., and Cox, P. M.: Detection of solar dimming and brightening effects on Northern Hemisphere river flow, Nature Geoscience, 7, 796–800, https://doi.org/10.1038/ngeo2263, 2014.

Gentine, P., Green, J. K., Guérin, M., Humphrey, V., Seneviratne, S. I., Zhang, Y., and Zhou, S.: Coupling between the terrestrial carbon and water cycles—a review, Environmental Research Letters, 14, 083 003, https://doi.org/10.1088/1748-9326/ab22d6, 2019.

Ghiggi, G., Humphrey, V., Seneviratne, S. I., and Gudmundsson, L.: GRUN: an observation-based global gridded runoff dataset from 1902 to 2014, Earth System Science Data, 11, 1655–1674, https://doi.org/10.5194/essd-11-1655-2019, 2019.

Gier, B. K., Schlund, M., Friedlingstein, P., Jones, C. D., Jones, C., Zaehle, S., and Eyring, V.: Representation of the terrestrial carbon cycle in CMIP6, Biogeosciences, 21, 5321–5360, https://doi.org/10.5194/bg-21-5321-2024, 2024.

Gleeson, T., Wang-Erlandsson, L., Porkka, M., Zipper, S. C., Jaramillo, F., Gerten, D., Fetzer, I., Cornell, S. E., Piemontese, L., Gordon, L. J., Rockström, J., Oki, T., Sivapalan, M., Wada, Y., Brauman, K. A., Flörke, M., Bierkens, M. F. P., Lehner, B., Keys, P., Kummu, M., Wagener, T., Dadson, S., Troy, T. J., Steffen, W., Falkenmark, M., and Famiglietti, J. S.: Illuminating water cycle modifications and Earth system resilience in the Anthropocene, Water Resources Research, 56, e2019WR024 957, https://doi.org/10.1029/2019WR024957, 2020a.

Gleeson, T., Wang-Erlandsson, L., Zipper, S. C., Porkka, M., Jaramillo, F., Gerten, D., Fetzer, I., Cornell, S. E., Piemontese, L., Gordon, L. J., Rockström, J., Oki, T., Sivapalan, M., Wada, Y., Brauman, K. A., Flörke, M., Bierkens, M. F. P., Lehner, B., Keys, P., Kummu, M., Wagener, T., Dadson, S., Troy, T. J., Steffen, W., Falkenmark, M., and Famiglietti, J. S.: The Water Planetary Boundary: Interrogation and Revision, One Earth, 2, 223–234, https://doi.org/10.1016/j.oneear.2020.02.009, 2020b.

Gnann, S., Baldwin, J. W., Cuthbert, M. O., Gleeson, T., Schwanghart, W., and Wagener, T.: The Influence of Topography on the Global Terrestrial Water Cycle, Reviews of Geophysics, 63, e2023RG000 810, https://doi.org/10.1029/2023RG000810, 2025.

Greve, P., Orlowsky, B., Mueller, B., Sheffield, J., Reichstein, M., and Seneviratne, S. I.: Global assessment of trends in wetting and drying over land, Nature Geoscience, 7, 716–721, https://doi.org/10.1038/ngeo2247, 2014.

Hajima, T., Watanabe, M., Yamamoto, A., Tatebe, H., Noguchi, M. A., Abe, M., Ohgaito, R., Ito, A., Yamazaki, D., Okajima, H., Ito, A., Takata, K., Ogochi, K., Watanabe, S., and Kawamiya, M.: Development of the MIROC-ES2L Earth system model and the evaluation of biogeochemical processes and feedbacks, Geoscientific Model Development, 13, 2197–2244, https://doi.org/10.5194/gmd-13-2197-2020, 2020.

Han, J., Yang, Y., Roderick, M. L., McVicar, T. R., Yang, D., Zhang, S., and Beck, H. E.: Assessing the Steady-State Assumption in Water Balance Calculation Across Global Catchments, Water Resources Research, 56, e2020WR027 392, https://doi.org/10.1029/2020WR027392, 2020.

Hausfather, Z. and Peters, G. P.: Emissions – the 'business as usual' story is misleading, Nature, 577, 618–620, https://doi.org/10.1038/d41586-020-00177-3, 2020.

He, M., Piao, S., Huntingford, C., Xu, H., Wang, X., Bastos, A., Cui, J., and Gasser, T.: Amplified warming from physiological responses to carbon dioxide reduces the potential of vegetation for climate change mitigation, Communications Earth & Environment, 3, 160, https://doi.org/10.1038/s43247-022-00489-4, 2022.

Horton, R. E.: The Role of infiltration in the hydrologic cycle, Eos, Transactions American Geophysical Union, 14, 446–460, https://doi.org/10.1029/TR014i001p00446, 1933.

Hou, Y., Guo, H., Yang, Y., and Liu, W.: Global Evaluation of Runoff Simulation From Climate, Hydrological and Land Surface Models, Water Resources Research, 59, e2021WR031 817, https://doi.org/10.1029/2021WR031817, 2023.

https://doi.org/10.5194/egusphere-2025-5896
Preprint. Discussion started: 4 December 2025

Hurtt, G. C., Chini, L., Sahajpal, R., Frolking, S., Bodirsky, B. L., Calvin, K., Doelman, J. C., Fisk, J., Fujimori, S., Klein Goldewijk, K., Hasegawa, T., Havlik, P., Heinimann, A., Humpenöder, F., Jungclaus, J., Kaplan, J. O., Kennedy, J., Krisztin, T., Lawrence, D., Lawrence, P., Ma, L., Mertz, O., Pongratz, J., Popp, A., Poulter, B., Riahi, K., Shevliakova, E., Stehfest, E., Thornton, P., Tubiello, F. N., van Vuuren, D. P., and Zhang, X.: Harmonization of global land use change and management for the period 850–2100 (LUH2) for CMIP6, Geoscientific Model Development, 13, 5425–5464, https://doi.org/10.5194/gmd-13-5425-2020, 2020.

Idso, S. B. and Brazel, A. J.: Rising atmospheric carbon dioxide concentrations may increase streamflow, Nature, 312, 51–53, https://doi.org/10.1038/312051a0, 1984.

Jackson, R. B., Jobbágy, E. G., Avissar, R., Roy, S. B., Barrett, D. J., Cook, C. W., Farley, K. A., le Maitre, D. C., McCarl, B. A., and Murray, B. C.: Trading Water for Carbon with Biological Carbon Sequestration, Science, 310, 1944–1947, https://doi.org/10.1126/science.1119282, 2005.

Keenan, T. F., Hollinger, D. Y., Bohrer, G., Dragoni, D., Munger, J. W., Schmid, H. P., and Richardson, A. D.: Increase in forest water-use efficiency as atmospheric carbon dioxide concentrations rise, Nature, 499, 324–327, https://doi.org/10.1038/nature12291, 2013.

Knoben, W. J. M., Woods, R. A., and Freer, J. E.: A Quantitative Hydrological Climate Classification Evaluated With Independent Streamflow Data, Water Resources Research, 54, 5088–5109, https://doi.org/10.1029/2018WR022913, 2018.

Leakey, A. D. B., Ainsworth, E. A., Bernacchi, C. J., Rogers, A., Long, S. P., and Ort, D. R.: Elevated CO2 effects on plant carbon, nitrogen, and water relations: six important lessons from FACE, Journal of Experimental Botany, 60, 2859–2876, https://doi.org/10.1093/jxb/erp096, 2009.

Lee, J.-E., Lintner, B. R., Neelin, J. D., Jiang, X., Gentine, P., Boyce, C. K., Fisher, J. B., Perron, J. T., Kubar, T. L., Lee, J., and Worden, J.: Reduction of tropical land region precipitation variability via transpiration, Geophysical Research Letters, 39, https://doi.org/10.1029/2012GL053417, 2012.

Li, J., Miao, C., Wei, W., Zhang, G., Hua, L., Chen, Y., and Wang, X.: Evaluation of CMIP6 Global Climate Models for Simulating Land Surface Energy and Water Fluxes During 1979–2014, Journal of Advances in Modeling Earth Systems, 13, e2021MS002 515, https://doi.org/10.1029/2021MS002515, 2021.

Lian, X., Piao, S., Chen, A., Huntingford, C., Fu, B., Li, L. Z. X., Huang, J., Sheffield, J., Berg, A. M., Keenan, T. F., McVicar, T. R., Wada, Y., Wang, X., Wang, T., Yang, Y., and Roderick, M. L.: Multifaceted characteristics of dryland aridity changes in a warming world, Nature Reviews Earth & Environment, 2, 232–250, https://doi.org/10.1038/s43017-021-00144-0, 2021.

Lundberg, S. M. and Lee, S.-I.: A Unified Approach to Interpreting Model Predictions, Advances in Neural Information Processing Systems, 30, https://doi.org/10.48550/arXiv.1705.07874, 2017.

Mankin, J. S., Smerdon, J. E., Cook, B. I., Williams, A. P., and Seager, R.: The Curious Case of Projected Twenty-First-Century Drying but Greening in the American West, Journal of Climate, 30, 8689–8710, https://doi.org/10.1175/JCLI-D-17-0213.1, 2017.

Mankin, J. S., Seager, R., Smerdon, J. E., Cook, B. I., Williams, A. P., and Horton, R. M.: Blue Water Trade-Offs With Vegetation in a CO2-Enriched Climate, Geophysical Research Letters, 45, 3115–3125, https://doi.org/10.1002/2018GL077051, 2018.

Mankin, J. S., Seager, R., Smerdon, J. E., Cook, B. I., and Williams, A. P.: Mid-latitude freshwater availability reduced by projected vegetation responses to climate change, Nature Geoscience, 12, 983–988, https://doi.org/10.1038/s41561-019-0480-x, 2019.

Mauritsen, T., Bader, J., Becker, T., Behrens, J., Bittner, M., Brokopf, R., Brovkin, V., Claussen, M., Crueger, T., Esch, M., Fast, I., Fiedler, S., Fläschner, D., Gayler, V., Giorgetta, M., Goll, D. S., Haak, H., Hagemann, S., Hedemann, C., Hohenegger, C., Ilyina, T., Jahns, T., Jimenéz-de-la Cuesta, D., Jungclaus, J., Kleinen, T., Kloster, S., Kracher, D., Kinne, S., Kleberg, D., Lasslop, G., Kornblueh, L., Marotzke, J., Matei, D., Meraner, K., Mikolajewicz, U., Modali, K., Möbis, B., Müller, W. A., Nabel, J. E. M. S., Nam, C. C. W., Notz,

https://doi.org/10.5194/egusphere-2025-5896
Preprint. Discussion started: 4 December 2025

D., Nyawira, S.-S., Paulsen, H., Peters, K., Pincus, R., Pohlmann, H., Pongratz, J., Popp, M., Raddatz, T. J., Rast, S., Redler, R., Reick, C. H., Rohrschneider, T., Schemann, V., Schmidt, H., Schnur, R., Schulzweida, U., Six, K. D., Stein, L., Stemmler, I., Stevens, B., von Storch, J.-S., Tian, F., Voigt, A., Vrese, P., Wieners, K.-H., Wilkenskjeld, S., Winkler, A., and Roeckner, E.: Developments in the MPI-M Earth System Model version 1.2 (MPI-ESM1.2) and Its Response to Increasing CO2, Journal of Advances in Modeling Earth Systems, 11, 998–1038, https://doi.org/10.1029/2018MS001400, 2019.

Milly, P. C. D. and Dunne, K. A.: Potential evapotranspiration and continental drying, Nature Climate Change, 6, 946–949, https://doi.org/10.1038/nclimate3046, 2016.

Milly, P. C. D. and Dunne, K. A.: Colorado River flow dwindles as warming-driven loss of reflective snow energizes evaporation, Science, 367, 1252–1255, https://doi.org/10.1126/science.aay9187, 2020.

Milly, P. C. D., Dunne, K. A., and Vecchia, A. V.: Global pattern of trends in streamflow and water availability in a changing climate, Nature, 438, 347–350, https://doi.org/10.1038/nature04312, 2005.

Miralles, D. G., Holmes, T. R. H., De Jeu, R. a. M., Gash, J. H., Meesters, A. G. C. A., and Dolman, A. J.: Global land-surface evaporation estimated from satellite-based observations, Hydrology and Earth System Sciences, 15, 453–469, https://doi.org/10.5194/hess-15-453-2011, 2011.

Muñoz-Sabater, J., Dutra, E., Agustí-Panareda, A., Albergel, C., Arduini, G., Balsamo, G., Boussetta, S., Choulga, M., Harrigan, S., Hersbach, H., Martens, B., Miralles, D. G., Piles, M., Rodríguez-Fernández, N. J., Zsoter, E., Buontempo, C., and Thépaut, J.-N.: ERA5-Land: a state-of-the-art global reanalysis dataset for land applications, Earth System Science Data, 13, 4349–4383, https://doi.org/10.5194/essd-13-4349-2021, 2021.

Nijssen, B., O'Donnell, G. M., Hamlet, A. F., and Lettenmaier, D. P.: Hydrologic Sensitivity of Global Rivers to Climate Change, Climatic Change, 50, 143–175, https://doi.org/10.1023/A:1010616428763, 2001.

Niu, G.-Y., Yang, Z.-L., Dickinson, R. E., and Gulden, L. E.: A simple TOPMODEL-based runoff parameterization (SIMTOP) for use in global climate models, Journal of Geophysical Research: Atmospheres, 110, https://doi.org/10.1029/2005JD006111, 2005.

Novák, V. and van Genuchten, M. T.: Using the transpiration regime to estimate biomass production, Soil Science, 173, 401, https://doi.org/10.1097/SS.0b013e318178e739, 2008.

Orth, R. and Destouni, G.: Drought reduces blue-water fluxes more strongly than green-water fluxes in Europe, Nature Communications, 9, 3602, https://doi.org/10.1038/s41467-018-06013-7, 2018.

Padrón, R. S., Gudmundsson, L., Liu, L., Humphrey, V., and Seneviratne, S. I.: Drivers of intermodel uncertainty in land carbon sink projections, Biogeosciences, 19, 5435–5448, https://doi.org/10.5194/bg-19-5435-2022, 2022.

Porkka, M., Virkki, V., Wang-Erlandsson, L., Gerten, D., Gleeson, T., Mohan, C., Fetzer, I., Jaramillo, F., Staal, A., te Wierik, S., Tobian, A., van der Ent, R., Döll, P., Flörke, M., Gosling, S. N., Hanasaki, N., Satoh, Y., Müller Schmied, H., Wanders, N., Famiglietti, J. S., Rockström, J., and Kummu, M.: Notable shifts beyond pre-industrial streamflow and soil moisture conditions transgress the planetary boundary for freshwater change, Nature Water, 2, 262–273, https://doi.org/10.1038/s44221-024-00208-7, 2024.

Riahi, K., Van Vuuren, D. P., Kriegler, E., Edmonds, J., O'Neill, B. C., Fujimori, S., Bauer, N., Calvin, K., Dellink, R., Fricko, O., Lutz, W., Popp, A., Cuaresma, J. C., Kc, S., Leimbach, M., Jiang, L., Kram, T., Rao, S., Emmerling, J., Ebi, K., Hasegawa, T., Havlik, P., Humpenöder, F., Da Silva, L. A., Smith, S., Stehfest, E., Bosetti, V., Eom, J., Gernaat, D., Masui, T., Rogelj, J., Strefler, J., Drouet, L., Krey, V., Luderer, G., Harmsen, M., Takahashi, K., Baumstark, L., Doelman, J. C., Kainuma, M., Klimont, Z., Marangoni, G., Lotze-Campen, H., Obersteiner, M., Tabeau, A., and Tavoni, M.: The Shared Socioeconomic Pathways and their energy, land use, and greenhouse

https://doi.org/10.5194/egusphere-2025-5896
Preprint. Discussion started: 4 December 2025

gas emissions implications: An overview, Global Environmental Change, 42, 153–168, https://doi.org/10.1016/j.gloenvcha.2016.05.009, 2017.

Richardson, K., Steffen, W., Lucht, W., Bendtsen, J., Cornell, S. E., Donges, J. F., Drüke, M., Fetzer, I., Bala, G., von Bloh, W., Feulner, G., Fiedler, S., Gerten, D., Gleeson, T., Hofmann, M., Huiskamp, W., Kummu, M., Mohan, C., Nogués-Bravo, D., Petri, S., Porkka, M., Rahmstorf, S., Schaphoff, S., Thonicke, K., Tobian, A., Virkki, V., Wang-Erlandsson, L., Weber, L., and Rockström, J.: Earth beyond six of nine planetary boundaries, Science Advances, 9, eadh2458, https://doi.org/10.1126/sciadv.adh2458, 2023.

Rockström, J. and Gordon, L.: Assessment of green water flows to sustain major biomes of the world: Implications for future ecohydrological landscape management, Physics and Chemistry of the Earth, Part B: Hydrology, Oceans and Atmosphere, 26, 843–851, https://doi.org/10.1016/S1464-1909(01)00096-X, 2001.

Rockström, J., Donges, J. F., Fetzer, I., Martin, M. A., Wang-Erlandsson, L., and Richardson, K.: Planetary Boundaries guide humanity's future on Earth, Nature Reviews Earth & Environment, 5, 773–788, https://doi.org/10.1038/s43017-024-00597-z, 2024.

Ruehr, S., Keenan, T. F., Williams, C., Zhou, Y., Lu, X., Bastos, A., Canadell, J. G., Prentice, I. C., Sitch, S., and Terrer, C.: Evidence and attribution of the enhanced land carbon sink, Nature Reviews Earth & Environment, 4, 518–534, https://doi.org/10.1038/s43017-023-00456-3, 2023.

Scheff, J., Coats, S., and Laguë, M. M.: Why do the Global Warming Responses of Land-Surface Models and Climatic Dryness Metrics Disagree?, Earth's Future, 10, e2022EF002 814, 2022.

Schneider, U., Hänsel, S., Finger, P., Rustemeier, E., and Ziese, M.: GPCC Full Data Monthly Product Version 2022 at 1.0°: Monthly Land-Surface Precipitation from Rain-Gauges built on GTS-based and Historical Data, Deutscher Wetterdienst, https://doi.org/10.5676/DWD_GPCC/CLIM_M_V2022_100, 2022.

Seland, O., Bentsen, M., Olivié, D., Toniazzo, T., Gjermundsen, A., Graff, L. S., Debernard, J. B., Gupta, A. K., He, Y.-C., Kirkevåg, A., Schwinger, J., Tjiputra, J., Aas, K. S., Bethke, I., Fan, Y., Griesfeller, J., Grini, A., Guo, C., Ilicak, M., Karset, I. H. H., Landgren, O., Liakka, J., Moseid, K. O., Nummelin, A., Spensberger, C., Tang, H., Zhang, Z., Heinze, C., Iversen, T., and Schulz, M.: Overview of the Norwegian Earth System Model (NorESM2) and key climate response of CMIP6 DECK, historical, and scenario simulations, Geoscientific Model Development, 13, 6165–6200, https://doi.org/10.5194/gmd-13-6165-2020, 2020.

Sellar, A. A., Jones, C. G., Mulcahy, J. P., Tang, Y., Yool, A., Wiltshire, A., O'Connor, F. M., Stringer, M., Hill, R., Palmieri, J., Woodward, S., de Mora, L., Kuhlbrodt, T., Rumbold, S. T., Kelley, D. I., Ellis, R., Johnson, C. E., Walton, J., Abraham, N. L., Andrews, M. B., Andrews, T., Archibald, A. T., Berthou, S., Burke, E., Blockley, E., Carslaw, K., Dalvi, M., Edwards, J., Folberth, G. A., Gedney, N., Griffiths, P. T., Harper, A. B., Hendry, M. A., Hewitt, A. J., Johnson, B., Jones, A., Jones, C. D., Keeble, J., Liddicoat, S., Morgenstern, O., Parker, R. J., Predoi, V., Robertson, E., Siahaan, A., Smith, R. S., Swaminathan, R., Woodhouse, M. T., Zeng, G., and Zerroukat, M.: UKESM1: Description and Evaluation of the U.K. Earth System Model, Journal of Advances in Modeling Earth Systems, 11, 4513–4558, https://doi.org/10.1029/2019MS001739, 2019.

Skinner, C. B., Poulsen, C. J., Chadwick, R., Diffenbaugh, N. S., and Fiorella, R. P.: The Role of Plant CO2 Physiological Forcing in Shaping Future Daily-Scale Precipitation, Journal of Climate, 30, 2319–2340, https://doi.org/10.1175/JCLI-D-16-0603.1, 2017.

Spracklen, D. V., Arnold, S. R., and Taylor, C. M.: Observations of increased tropical rainfall preceded by air passage over forests, Nature, 489, 282–285, https://doi.org/10.1038/nature11390, 2012.

Stein, L., Mukkavilli, S. K., Pfitzmann, B. M., Staar, P. W. J., Ozturk, U., Berrospi, C., Brunschwiler, T., and Wagener, T.: Wealth Over Woe: Global Biases in Hydro-Hazard Research, Earth's Future, 12, e2024EF004 590, https://doi.org/10.1029/2024EF004590, 2024.

https://doi.org/10.5194/egusphere-2025-5896
Preprint. Discussion started: 4 December 2025

Swann, A. L. S., Hoffman, F. M., Koven, C. D., and Randerson, J. T.: Plant responses to increasing CO2 reduce estimates of climate impacts on drought severity, Proceedings of the National Academy of Sciences, 113, 10 019–10 024, https://doi.org/10.1073/pnas.1604581113, 2016.

Swart, N. C., Cole, J. N. S., Kharin, V. V., Lazare, M., Scinocca, J. F., Gillett, N. P., Anstey, J., Arora, V., Christian, J. R., Hanna, S., Jiao, Y., Lee, W. G., Majaess, F., Saenko, O. A., Seiler, C., Seinen, C., Shao, A., Sigmond, M., Solheim, L., von Salzen, K., Yang, D., and Winter, B.: The Canadian Earth System Model version 5 (CanESM5.0.3), Geoscientific Model Development, 12, 4823–4873, https://doi.org/10.5194/gmd-12-4823-2019, 2019.

Séférian, R., Nabat, P., Michou, M., Saint-Martin, D., Voldoire, A., Colin, J., Decharme, B., Delire, C., Berthet, S., Chevallier, M., Sénési, S., Franchisteguy, L., Vial, J., Mallet, M., Joetzjer, E., Geoffroy, O., Guérémy, J.-F., Moine, M.-P., Msadek, R., Ribes, A., Rocher, M., Roehrig, R., Salas-y Mélia, D., Sanchez, E., Terray, L., Valcke, S., Waldman, R., Aumont, O., Bopp, L., Deshayes, J., Éthé, C., and Madec, G.: Evaluation of CNRM Earth System Model, CNRM-ESM2-1: Role of Earth System Processes in Present-Day and Future Climate, Journal of Advances in Modeling Earth Systems, 11, 4182–4227, https://doi.org/10.1029/2019MS001791, 2019.

Tabari, H.: Climate change impact on flood and extreme precipitation increases with water availability, Scientific Reports, 10, 13 768, https://doi.org/10.1038/s41598-020-70816-2, 2020.

Trenberth, K. E.: Conceptual Framework for Changes of Extremes of the Hydrological Cycle with Climate Change, Climatic Change, 42, 327–339, https://doi.org/10.1023/A:1005488920935, 1999.

Trenberth, K. E.: Changes in precipitation with climate change, Climate Research, 47, 123–138, https://doi.org/10.3354/cr00953, 2011.

Ukkola, A. M., Prentice, I. C., Keenan, T. F., van Dijk, A. I. J. M., Viney, N. R., Myneni, R. B., and Bi, J.: Reduced streamflow in water-stressed climates consistent with CO2 effects on vegetation, Nature Climate Change, 6, 75–78, https://doi.org/10.1038/nclimate2831, 2016.

Voldoire, A., Saint-Martin, D., Sénési, S., Decharme, B., Alias, A., Chevallier, M., Colin, J., Guérémy, J.-F., Michou, M., Moine, M.-P., Nabat, P., Roehrig, R., Salas y Mélia, D., Séférian, R., Valcke, S., Beau, I., Belamari, S., Berthet, S., Cassou, C., Cattiaux, J., Deshayes, J., Douville, H., Ethé, C., Franchistéguy, L., Geoffroy, O., Lévy, C., Madec, G., Meurdesoif, Y., Msadek, R., Ribes, A., Sanchez-Gomez, E., Terray, L., and Waldman, R.: Evaluation of CMIP6 DECK Experiments With CNRM-CM6-1, Journal of Advances in Modeling Earth Systems, 11, 2177–2213, https://doi.org/10.1029/2019MS001683, 2019.

Wada, Y., van Beek, L. P. H., and Bierkens, M. F. P.: Modelling global water stress of the recent past: on the relative importance of trends in water demand and climate variability, Hydrology and Earth System Sciences, 15, 3785–3808, https://doi.org/10.5194/hess-15-3785-2011, 2011.

Wada, Y., Flörke, M., Hanasaki, N., Eisner, S., Fischer, G., Tramberend, S., Satoh, Y., van Vliet, M. T. H., Yillia, P., Ringler, C., Burek, P., and Wiberg, D.: Modeling global water use for the 21st century: the Water Futures and Solutions (WFaS) initiative and its approaches, Geoscientific Model Development, 9, 175–222, https://doi.org/10.5194/gmd-9-175-2016, 2016.

Wada, Y., Bierkens, M. F. P., de Roo, A., Dirmeyer, P. A., Famiglietti, J. S., Hanasaki, N., Konar, M., Liu, J., Müller Schmied, H., Oki, T., Pokhrel, Y., Sivapalan, M., Troy, T. J., van Dijk, A. I. J. M., van Emmerik, T., Van Huijgevoort, M. H. J., Van Lanen, H. A. J., Vörösmarty, C. J., Wanders, N., and Wheater, H.: Human–water interface in hydrological modelling: current status and future directions, Hydrology and Earth System Sciences, 21, 4169–4193, https://hess.copernicus.org/articles/21/4169/2017/, 2017.

Wagener, T., Reinecke, R., and Pianosi, F.: On the evaluation of climate change impact models, WIREs Climate Change, 13, e772, https://doi.org/10.1002/wcc.772, 2022.

https://doi.org/10.5194/egusphere-2025-5896
Preprint. Discussion started: 4 December 2025

Wang, Y., Hu, J., Li, R., Song, B., Hailemariam, M., Fu, Y., and Duan, J.: Increasing Cloud Coverage Deteriorates Evapotranspiration Estimating Accuracy From Satellite, Reanalysis and Land Surface Models Over East Asia, Geophysical Research Letters, 50, e2022GL102 706, https://doi.org/10.1029/2022GL102706, 2023.

Wang-Erlandsson, L., Tobian, A., van der Ent, R. J., Fetzer, I., te Wierik, S., Porkka, M., Staal, A., Jaramillo, F., Dahlmann, H., Singh, C., Greve, P., Gerten, D., Keys, P. W., Gleeson, T., Cornell, S. E., Steffen, W., Bai, X., and Rockström, J.: A planetary boundary for green water, Nature Reviews Earth & Environment, 3, 380–392, https://doi.org/10.1038/s43017-022-00287-8, 2022.

Wei, H., Zhang, Y., Huang, Q., Chiew, F. H. S., Luan, J., Xia, J., and Liu, C.: Direct vegetation response to recent CO2 rise shows limited effect on global streamflow, Nature Communications, 15, 9423, https://doi.org/10.1038/s41467-024-53879-x, 2024.

Wei, H., Zhang, Y., Huang, Q., Liu, C., and Wagener, T.: Functional Relationships Reveal Large Differences in Streamflow Response to eCO2-Vegetation in Global Water Models, Geophysical Research Letters, 52, e2024GL113 685, https://doi.org/10.1029/2024GL113685, 2025.

Weiskel, P. K., Wolock, D. M., Zarriello, P. J., Vogel, R. M., Levin, S. B., and Lent, R. M.: Hydroclimatic regimes: a distributed water-balance framework for hydrologic assessment, classification, and management, Hydrology and Earth System Sciences, 18, 3855–3872, https://doi.org/10.5194/hess-18-3855-2014, 2014.

Wu, R.-J., Lo, M.-H., and Scanlon, B. R.: The Annual Cycle of Terrestrial Water Storage Anomalies in CMIP6 Models Evaluated against GRACE Data, Journal of Climate, 34, 8205–8217, https://doi.org/10.1175/JCLI-D-21-0021.1, 2021.

Wu, T., Lu, Y., Fang, Y., Xin, X., Li, L., Li, W., Jie, W., Zhang, J., Liu, Y., Zhang, L., Zhang, F., Zhang, Y., Wu, F., Li, J., Chu, M., Wang, Z., Shi, X., Liu, X., Wei, M., Huang, A., Zhang, Y., and Liu, X.: The Beijing Climate Center Climate System Model (BCC-CSM): the main progress from CMIP5 to CMIP6, Geoscientific Model Development, 12, 1573–1600, https://doi.org/10.5194/gmd-12-1573-2019, 2019.

Yang, H., Piao, S., Huntingford, C., Ciais, P., Li, Y., Wang, T., Peng, S., Yang, Y., Yang, D., and Chang, J.: Changing the retention properties of catchments and their influence on runoff under climate change, Environmental Research Letters, 13, 094 019, https://doi.org/10.1088/1748-9326/aadd32, 2018.

Yang, Y., McVicar, T. R., Yang, D., Zhang, Y., Piao, S., Peng, S., and Beck, H. E.: Low and contrasting impacts of vegetation CO_2 fertilization on global terrestrial runoff over 1982–2010: accounting for aboveground and belowground vegetation–CO_2 effects, Hydrology and Earth System Sciences, 25, 3411–3427, https://doi.org/10.5194/hess-25-3411-2021, 2021.

Yang, Y., Roderick, M. L., Guo, H., Miralles, D. G., Zhang, L., Fatichi, S., Luo, X., Zhang, Y., McVicar, T. R., Tu, Z., Keenan, T. F., Fisher, J. B., Gan, R., Zhang, X., Piao, S., Zhang, B., and Yang, D.: Evapotranspiration on a greening Earth, Nature Reviews Earth & Environment, 4, 626–641, https://doi.org/10.1038/s43017-023-00464-3, 2023.

Yin, J., Gentine, P., Zhou, S., Sullivan, S. C., Wang, R., Zhang, Y., and Guo, S.: Large increase in global storm runoff extremes driven by climate and anthropogenic changes, Nature Communications, 9, 4389, https://doi.org/10.1038/s41467-018-06765-2, 2018.

Zhang, Y., Zheng, H., Zhang, X., Leung, L. R., Liu, C., Zheng, C., Guo, Y., Chiew, F. H. S., Post, D., Kong, D., Beck, H. E., Li, C., and Blöschl, G.: Future global streamflow declines are probably more severe than previously estimated, Nature Water, 1, 261–271, https://doi.org/10.1038/s44221-023-00030-7, 2023.

Zhao, Q., Zhu, Z., Zeng, H., Zhao, W., and Myneni, R. B.: Future greening of the Earth may not be as large as previously predicted, Agricultural and Forest Meteorology, 292-293, 108 111, https://doi.org/10.1016/j.agrformet.2020.108111, 2020.

Zheng, H., Yang, Z.-L., Lin, P., Wei, J., Wu, W.-Y., Li, L., Zhao, L., and Wang, S.: On the Sensitivity of the Precipitation Partitioning Into Evapotranspiration and Runoff in Land Surface Parameterizations, Water Resources Research, 55, 95–111, https://doi.org/10.1029/2017WR022236, 2019.

https://doi.org/10.5194/egusphere-2025-5896
Preprint. Discussion started: 4 December 2025

Zhu, Z., Piao, S., Myneni, R. B., Huang, M., Zeng, Z., Canadell, J. G., Ciais, P., Sitch, S., Friedlingstein, P., Arneth, A., Cao, C., Cheng, L., Kato, E., Koven, C., Li, Y., Lian, X., Liu, Y., Liu, R., Mao, J., Pan, Y., Peng, S., Peñuelas, J., Poulter, B., Pugh, T. A. M., Stocker, B. D., Viovy, N., Wang, X., Wang, Y., Xiao, Z., Yang, H., Zaehle, S., and Zeng, N.: Greening of the Earth and its drivers, Nature Climate Change, 6, 791–795, https://doi.org/10.1038/nclimate3004, 2016.